

1 Characterization of the epitranscriptomic landscape of HIV-infected cells

2
3 Sara Cristinelli*¹, Paolo Angelino*², Andrew Janowczyk², Mauro Delorenzi^{2,3}, Angela Ciuffi¹

4 ¹*Institute of Microbiology, Lausanne University Hospital and University of Lausanne, CH-1011 Lausanne, Switzerland.*

5 ²*BCF - Bioinformatics Core Facility, SIB Swiss Institute of Bioinformatics, Lausanne, CH-1015 Switzerland.*

6 ³*TBS - Translational bioinformatics and statistics, Department of Oncology, University of Lausanne, CH-1011*
7 *Lausanne, Switzerland.*

8 * These authors contributed equally to this work
9

10 Abstract

11 The study of RNA modifications, today known as epitranscriptomics, is of growing interest. The N6-
12 methyladenosine (m⁶A) and 5-methylcytosine (m⁵C) RNA modifications are abundantly present on mRNA
13 molecules, and impact RNA interactions with other proteins or molecules, thereby affecting cellular
14 processes, such as RNA splicing, export, stability and translation. Recently m⁶A and m⁵C marks were found
15 to be present on human immunodeficiency (HIV) transcripts as well and affect viral replication. Therefore,
16 the discovery of RNA methylation provides a new layer of regulation of HIV expression and replication,
17 and thus offers novel array of opportunities to inhibit replication. However, no study has been performed
18 to date to investigate the impact of HIV replication on the transcript methylation level in the infected cell.
19 We used a productive HIV infection model, consisting of the CD4+ SupT1 T cell line infected with a VSV-G
20 pseudotyped HIVeGFP-based vector, to explore the temporal landscape of m⁶A and m⁵C epitranscriptomic
21 marks upon HIV infection, and compare it to mock-treated cells. Cells were collected at 12, 24 and 36h
22 post-infection for mRNA extraction and FACS analysis. M⁶A RNA modifications were investigated by
23 methylated RNA immunoprecipitation followed by high-throughput sequencing (MeRIP-Seq). M⁵C RNA
24 modifications were investigated using a bisulfite conversion approach followed by high-throughput
25 sequencing (BS-Seq).

26 Our data suggest that HIV Infection impacted the methylation landscape of HIV-infected cells, inducing
27 mostly increased methylation of cellular transcripts upon infection. Indeed, differential methylation (DM)
28 analysis identified 59 m⁶A hypermethylated and only 2 hypomethylated transcripts and 14 m⁵C
29 hypermethylated transcripts and 7 hypomethylated ones. Furthermore, both m⁶A and m⁵C methylations
30 were detected on viral transcripts and viral particle RNA genomes, as previously described, but additional
31 patterns were identified.

32 This work used differential epitranscriptomic analysis to identify novel players involved in HIV life cycle,
33 thereby providing innovative opportunities for HIV regulation.
34
35

36 Introduction

37 The presence of chemical modifications along RNA molecules has been known since the 70s (1). Only
38 recently, however, new technologies allowed the identification and investigation of chemical
39 modifications at transcriptome-wide level, allowing mapping of some modifications in mRNA (2, 3). Similar
40 to epigenetics that focuses on the understanding of DNA and histone modifications in the regulation of
41 transcription, epitranscriptomics investigates RNA modifications and offers a new layer of regulation,
42 impacting and tuning cellular processes, including RNA splicing, export, stability and translation (4).
43 Among these modifications N⁶-methyladenosine (m⁶A) and 5-methylcytosine (m⁵C) are found to be
44 particularly abundant along mRNA molecules (5).

45 Regulation of RNA modifications is under the control of specific cellular proteins (6, 7). The methylases
46 METTL3-14 together with adaptor proteins act as m⁶A writer complexes of mRNA and catalyze the
47 methylation of adenosine residues within the consensus motif DRA*CH (D = G/A/U, R = G/A, H = U/A/C,
48 and A* = modified A). RNA binding proteins act as m⁶A readers, they bind methylated residues, thereby
49 modulating the fate and metabolism of marked mRNA, *i.e.* secondary structure, nuclear export, stability,
50 splicing, and degradation. Demethylases such as ALKBH5 act as erasers of m⁶A, removing the chemical
51 modification from transcripts.

52 The role and identity of proteins involved in m⁵C turnover is less clear. The addition of m⁵C residues on
53 mRNA molecules is carried out by the methylase NSUN2. M⁵C binding proteins seem to play a role in
54 export and degradation, while to date no m⁵C-specific demethylase has been described yet.

55 The role of RNA modifications is not limited to cellular RNA molecules. Indeed, recent studies highlighted
56 the importance of RNA methylation on viral transcripts as well, including human immunodeficiency virus
57 type 1 (HIV-1, hereafter abbreviated HIV) RNA, and its impact in regulating viral replication and gene
58 expression.

59 Lichinchi *et al.* reported 14 peaks of m⁶A modification in HIV RNA, including a m⁶A peak in the Rev
60 response-element (RRE) region (8). They showed that RRE methylation increased Rev binding and
61 facilitated nuclear export of viral RNA, thereby enhancing HIV replication. Kennedy *et al.* found four
62 clusters of m⁶A modifications in the 3' Untranslated region (UTR) of HIV RNA and suggested that the
63 overexpression of the m⁶A readers YTDHF1-3 likely stabilize viral mRNAs, thereby increasing viral
64 replication (9). In contrast, Tirumuru *et al.* and Lu *et al.* showed that HIV RNA has m⁶A modifications in
65 both 5' and 3' UTRs, as well as in *gag* and *rev* genes, and that overexpression of YTDHF1-3 proteins in cells
66 inhibits HIV infection by decreasing viral genomic RNA (gRNA) and early reverse transcription products
67 (10, 11).

68 A recent study from Courtney *et al.* investigate the role of m⁵C in HIV replication (12). Using an antibody-
69 based capture approach, they identified m⁵C-methylated residues in HIV gRNA from CEM T cell-derived
70 virions and on cellular HIV transcripts. They identified the m⁵C mRNA writer NSUN2 as the writer
71 responsible for HIV RNA m⁵C methylation and demonstrated a role of m⁵C in favoring alternative splicing
72 and increasing HIV mRNA translation.

73 Furthermore, it has been reported that upon HIV infection, the global cellular rate of m⁶A and m⁵C
74 methylation increased (12, 13). However, an in-depth exploration of the differentially methylated genes
75 upon HIV infection is missing.

76 The discovery of HIV RNA methylation provides a new layer of regulation of HIV expression and replication,
77 and thus a novel array of opportunities to inhibit replication. Investigating the epitranscriptomic landscape
78 of HIV-infected cells will lead to a deeper understanding of HIV-induced RNA modifications and may help
79 to identify novel host cells factors, HIV dependency factors (HDF) or restriction factors (HRF), involved in
80 HIV replication. Indeed, HIV may modulate HDF and HRF to impact viral replication efficiency not only at
81 the level of transcription but also at the level of methylation.

82 Here we used the SupT1 CD4+ T cellular model infected with a VSV.G pseudotyped HIV-based vector
83 encoding a GFP reporter (HIVeGFP) to explore the m⁶A and m⁵C modification pattern of cellular and viral
84 transcripts in HIV-infected cells, as well as the virion genomic RNA, over time. We found that HIV Infection
85 impacted the methylation landscape of HIV-infected cells by inducing an increased proportion of
86 methylated cellular transcripts. Differential methylation (DM) analysis allowed identifying a few genes
87 that may act as HDF or HRF and thus impact viral replication success. Furthermore, both m⁶A and m⁵C
88 methylation was detected on viral transcripts and on viral particle packaged RNA genome, as previously
89 described, but additional patterns were also detected.

90

91

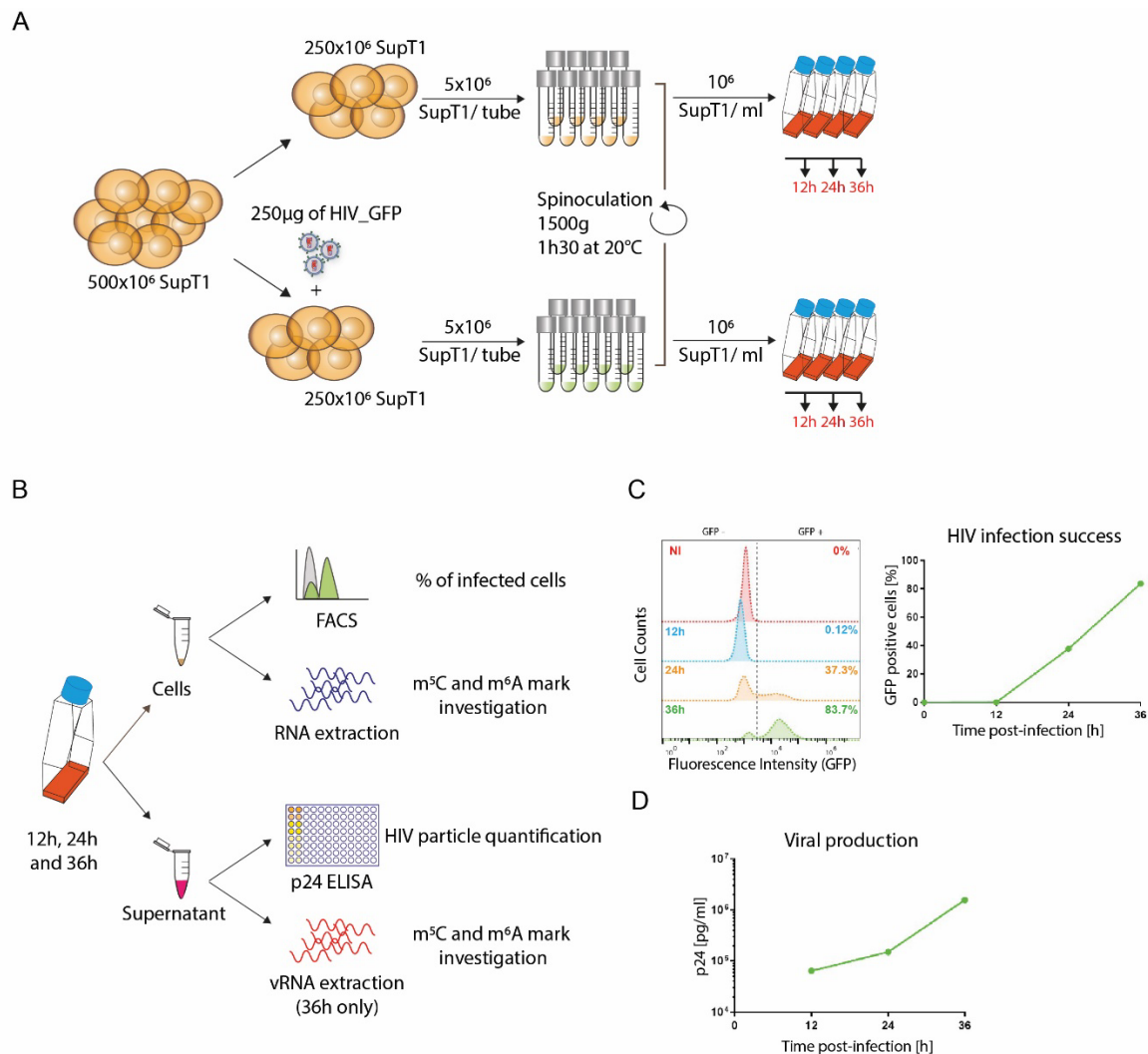
92 **Results**

93 **Dynamic analysis of HIV-infected cells**

94 To explore the transcriptomic and epitranscriptomic landscape of HIV-infected cells, we infected SupT1
95 cells (a CD4+ T-cell-line) with an HIV_GFP-based vector. At 12h, 24h and 36h post-infection, we (i) assessed
96 the percentage of infected cells, monitoring GFP expression by FACS analysis; (ii) measured the amount
97 of viral particles released in the supernatant and (iii) extracted the total RNA, purified polyA RNA and
98 explored the m⁶A and m⁵C landscapes, by either methylated RNA immunoprecipitation sequencing
99 (MeRIP-Seq) or Bisulfite sequencing (BS-Seq) respectively (Figure 1A-B).

100 Infection success was monitored over time, following the accumulation of the virally-encoded GFP
101 protein. At 12h post-infection (p.i.), as expected, the GFP expression was not yet detectable, while at 24h
102 p.i. 37.3% of the cells were expressing detectable levels of GFP and 83.7% of the cells were GFP+ at 36h
103 p.i., close to universal infection (Figure 1C). These results were consistent with viral particle production
104 assessed by p24 measurement, which showed increasing viral production over time, with 0.064×10^6
105 pg/ml at 12 h p.i., 0.150×10^6 pg/ml at 24h p.i. and 1.572×10^6 pg/ml at 36h p.i. (Figure 1D).

106



107

108 **Figure 1. Dynamic analysis of HIV-infected cells. (A)** Infection setting overview. SupT1 cells were either infected
 109 with 1 µg/10⁶ cells p24 equivalent of HIV_GFP virus or left uninfected, divided into aliquots of 5*10⁶ cells/ tube and
 110 spinoculated for 90 minutes at 1500 g and 20°C to allow nearly universal infection. Cells were then resuspended at
 111 a concentration of 10⁶ cells/ml and further incubated. **(B)** Experimental design overview. At 12, 24 and 36h post-
 112 infection, viral supernatant was collected to assess viral production by p24 ELISA; 300.000 cells were fixed and HIV
 113 infection success was assessed by evaluating HIV-encoded GFP expression by FACS analysis; the rest of the cells was
 114 used for RNA extraction and further analyses on m⁶A and m⁵C epitranscriptomic marks. **(C)** Example of FACS analysis
 115 at 12h, 24h and 36h post-infection to evaluate HIV infection success. Left: Histogram plots of FACS analyses showing
 116 the GFP intensity (x-axis) on the different samples, non-infected (NI) and infected (12h, 24h, 36h) samples. Right:
 117 Graphical representation of the proportion of infected cells (%GFP-positive cells) **(D)** Example of p24 ELISA to
 118 monitor viral particle production. Results are expressed as pg of p24 per ml of supernatant over time.

119

120 HIV infection induced changes at gene expression level

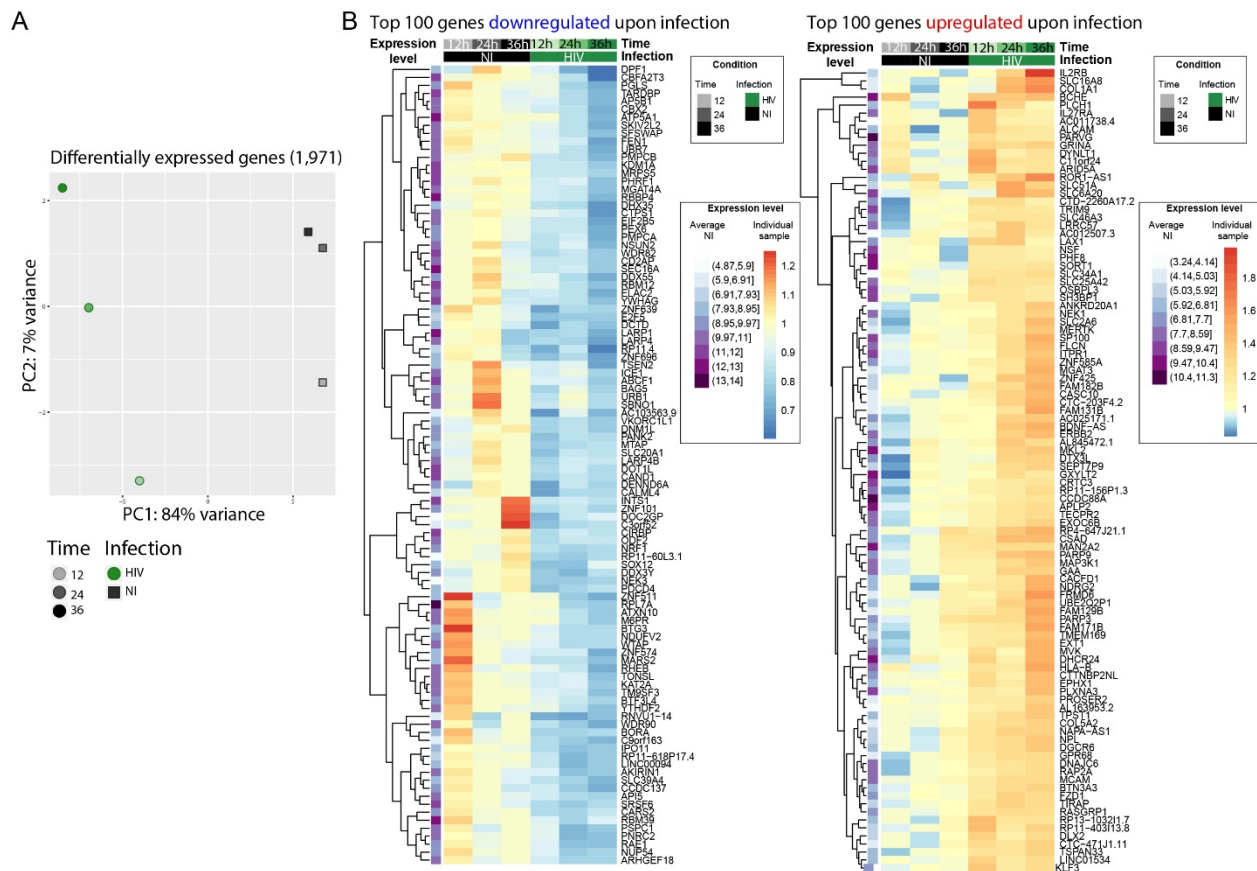
121 Transcriptome analysis was performed by RNA-Seq on polyA-selected RNAs over time on infected (HIV)
 122 and non-infected mock (NI) SupT1 cells. Altogether, a total of 17,676 genes out of 58,136 were detected

123 (12h NI: 11,908; 12h HIV: 10,980; 24h NI: 13,516; 24h HIV: 12,327; 36h NI: 15,004; 36h HIV: 11,827). In
124 order to increase the specificity of our study we applied a supplemental filter to retain genes above 3
125 counts per million (CPM). This filter was applied to each condition (Infected or non-infected) individually
126 in order to avoid the introduction of bias upon differential gene expression analyses. Upon quality control
127 and filtering, a total of 13,103 genes was retained for further analysis (Table S1).

128 Principal component (PC) analyses separated samples in 2 distinct clusters according to infection condition
129 and time progression, with the PC1 and PC2 representing respectively 67% and 21% of the variance (Figure
130 S1A). Such clustering was not due to the presence of HIV transcripts, as upon their removal, sample
131 distribution was maintained (Figure S1B). Among the 13,103 detected genes, 1,654 (13%) were
132 overexpressed over time while 2,142 (16%) were downregulated. Analysis over time of NI samples only
133 revealed that some genes were differentially expressed, likely due to cell culture conditions and cell
134 growth, but independently from HIV infection (Table S1). In order to refine the analysis and to observe
135 the *bona fide* impact of HIV infection, the time effect was modeled in a linear model and subtracted to
136 the HIV effect, resulting in improved defined variance (Figure S1C). Thus, upon removal of the time effect,
137 HIV infection alone modulated a total of 1,971 genes, upregulating 813 genes (6.2%) and downregulating
138 1,158 genes (8.8%) (Table S1 and Figure 2). Gene ontology analysis shows that the 1,971 differentially
139 expressed genes were enriched in the negative regulation of biological and cellular. These data are
140 consistent with our previous study, performed using similar experimental conditions, revealing >75%
141 concordance, and arguing for some degree of reproducibility and confidence (data not shown) (14).

142 Overall, these data confirmed that HIV induced numerous changes at transcriptome level upon infection,
143 that need to be taken into account for an accurate exploration of the epitranscriptomic landscape. Indeed,
144 methylated genes that are strongly impacted by HIV in term of gene expression may introduce a bias to
145 the analysis, *i.e* methylated genes overexpressed upon infection may be considered also as differentially
146 methylated if no correction is applied.

147 Hence, in order to explore the m⁶A and m⁵C epitranscriptomic landscape of HIV-infected cells
148 independently from their expression level upon infection, all data were normalized to the corresponding
149 gene expression.



150

151 **Figure 2. HIV infection induced changes at gene expression level. (A)** PCA representing 1,971 differentially
 152 expressed genes upon HIV infection only. HIV-infected samples (HIV) are represented as green filled circles, non-
 153 infected samples (NI) as grey filled squares. Timepoints are depicted by the shade of the color. Time effect has been
 154 removed, HIV transcripts are not included. **(B)** Heatmaps of the top 100 (out of 813) downregulated (left) or top 100
 155 (out of 1,158) upregulated (right) genes upon HIV infection. The first column (purple) represents the average gene
 156 expression of each gene in the 3 normalized NI samples together, i.e. the darker the color, the higher the expression
 157 in the time-averaged NI gene expression. The log fold change of each gene compared to the average NI gene expression
 158 is depicted in shades of blue to red.

159

160 HIV infection induced changes in cellular m⁶A profile

161 We examined the landscape of the m⁶A RNA methylome during HIV infection at 12h, 24h and 36h post-
 162 infection by MeRIP-Seq using either an m⁶A specific antibody or a non-specific IgG antibody as control
 163 (15). After pull down and elution, quality and quantity of samples were verified on a fragment analyzer
 164 (Figure S2A). The immunoprecipitated RNA was used for library preparation and sequencing; of note, the
 165 amount of RNA retrieved from the control condition was too low to perform library preparation and
 166 sequencing.

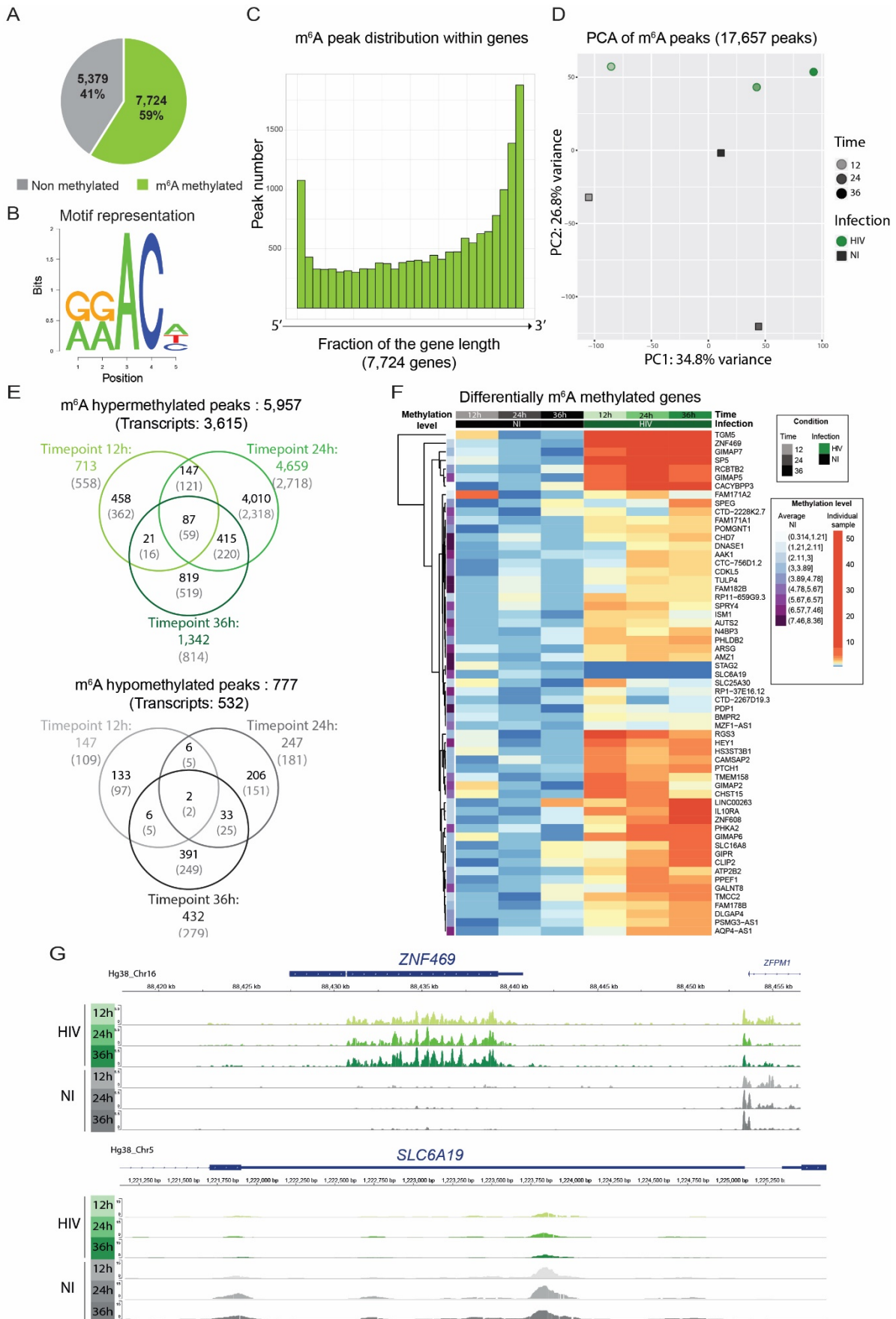
167 We obtained a range of 26-72 million reads per condition (Figure S2). After quality control and filtering, 8
 168 to 46 million clean reads were kept and further mapped to the HIV and hg38 human genomes, with
 169 alignment success typically exceeding 99%.

170 m⁶A modified regions were identified using the peak calling package MACS2. A total of 17,657 peaks
171 mapping on 7,724 genes across all samples were retrieved representing 59% of the overall detected genes
172 (13,101) (Figure 3A and Table S2). We looked for the presence of the m⁶A consensus motif DRACH
173 previously identified and detected it in 17,527 peaks out of 17,657 (99.3% of the peaks) (Figure 3B) (5).
174 We further analyzed the 17,527 m⁶A peaks to identify, independently, additional consensus sequences
175 for m⁶A methylation. For this, 20 nucleotides surrounding the center of each m⁶A peak were examined
176 for motif retrieval, and revealed 2 additional highly enriched motifs, WGGAM and GSAGGAGG (Figure
177 S3A); these motifs have been previously described as m⁶A binding motifs from Zhang et al.(16). As described
178 previously, m⁶A peaks were globally enriched toward the 3' end of transcripts, and this distribution is not
179 altered upon HIV infection (Figures 3C and S3B) (17). M⁶A modifications were reported to be enriched in
180 long exons (>140 nt), however, upon normalization for exon width, we could not observe significant
181 changes in m⁶A distribution with only a slight enrichment in m⁶A peak frequency in exons >500nt (Figure
182 S3C)(17). Upon PC analysis of the m⁶A peaks retrieved in all samples, we could observe a separation
183 according to time and infection condition, suggesting an impact of HIV infection on the m⁶A methylation
184 profile (Figure 3C).

185 As m⁶A methylation can occur at different sites along the mRNA molecule, analysis was performed on
186 differentially methylated peaks. A total of 5,957 peaks corresponding to 3,615 transcripts, were found as
187 being hypermethylated upon HIV infection, with 713 peaks at 12h; 4,696 at 24h and 1,342 at 36h post
188 infection (corresponding to 558, 2,718 and 814 transcripts at 12h, 24h and 36h respectively). Only 777
189 hypomethylated peaks (532 transcripts) were identified, with 147, 247 and 432 peaks at 12h, 24h, 36h
190 post infection, corresponding respectively to 109 transcripts at 12h, 181 at 24h and 279 at 36h post
191 infection (Table S3 and Figure 3D).

192 We identified 87 m⁶A peaks, representing 59 different transcripts that were commonly hypermethylated
193 in infected cells at 12h, 24h and 36h post-infection. However, only 2 peaks, identified as the stromal
194 antigen 1 (STAG1) and the solute carrier family 6 member 19 (SLC6A19) respectively, were found to be
195 commonly hypomethylated upon infection at the 3 timepoints (Table S2 and Figure 3D to F). Gene
196 ontology analysis of the 61 commonly differentially methylated mRNAs did not reveal any statistically
197 significant enrichment in biological process (data not shown). However, we noticed the presence of 4 out
198 of the 7 GTPase Immuno-Associated Proteins (GIMAP) within the
199 commonly differentially methylated transcripts and overall 6 GIMAPs among the totality of the
200 differentially methylated transcripts (GIMAP1, GIMAP2, GIMAP4, GIMAP5, GIMAP6, GIMAP7). GIMAPs

201 are involved in response to pathogens and have a prominent role in T cell survival and differentiation,
202 consistent with a putative role of these genes on HIV replication (18).



204

205 **Figure 3: HIV infection induced changes in cellular m⁶A profile.** (A) Pie-Chart representing the proportion of m⁶A
206 methylated transcripts among the totality of detected transcripts (13,103). (B) Representation of the enriched m⁶A
207 DRACH motif among the samples. (C) Histogram plots showing on the x-
208 axis genes normalized for their length and divided into 30 bins, and for each bin fraction of the gene, the number of
209 m⁶A residues. (D) PCA of the variance of m⁶A peaks among all samples. HIV-infected samples are represented as
210 green filled circles, non-infected samples as grey filled squares. Timepoints are depicted by the shade of the color.
211 HIV transcripts are not included. (E) Venn-Diagrams showing hypermethylated (upper panel) or hypomethylated
212 (lower panel) m⁶A peaks upon infection. Values in black represent the number of m⁶A methylated peaks, values in
213 grey into brackets represent the number of corresponding transcripts (F) Heatmap of the commonly hyper/hypo
214 methylated transcripts upon infection at the three timepoints. The 61 differentially methylated genes are shown.
215 The average methylation level of the non-infected cells is represented in violet in the first column, and was used for
216 normalization. Differential methylation was then normalized to the average methylation intensity of each transcript.
217 (G) Examples of an hypermethylated (upper panel) and an hypomethylated (lower panel) transcript showing m⁶A
218 peak intensity and distribution across samples using IGV viewer.

219

220 HIV infection induced changes in cellular m⁵C profile

221 To obtain a transcriptome-wide landscape of m⁵C profiles, we performed BS-Seq on RNA samples purified
222 from HIV-GFP infected and non-infected SupT1 cells (19). Compared to antibody-based techniques,
223 bisulfite conversion allows higher resolution and higher sensitivity, identifying converted and non-
224 converted cytosines at single nucleotide resolution and providing estimations of the methylation rate of
225 each C residue. To assess efficiency of bisulfite conversion treatment, we used the human 28S rRNA as
226 positive control. Indeed, the C4447 residue of this rRNA is known to be methylated with a frequency of
227 100%.

228 Therefore, we spiked-in polyA-depleted RNA in each sample to ensure rRNA representation and presence
229 of 28S rRNA in particular. After bisulfite conversion, a sample aliquot was used for RT-PCR and Sanger
230 sequencing of the C4447 encompassing region of the 28S rRNA (Figure S4A). For all samples we observed
231 a complete C-T conversion along the fragment suggesting the absence of methylation on these C residues,
232 except for the C4447 residue that remains unchanged, confirming the methylation status of this specific
233 C residue (Figure S4B).

234 After library preparation and high-throughput sequencing we obtained a range of 23-43 million
235 reads/sample (Figure S4C) with a low representation of C and an over-representation of T, consistent with
236 successful unmethylated C-to-T bisulfite conversion (Figure S4D). Reads were processed with the meRan-
237 TK package, specific for RNA bisulfite conversion, taking into account the converted reads to allow genome
238 alignment and mapping (20).

239 To further assess the conversion rate in each sample, we also included a commercially available pool of
240 non-methylated RNA sequences (ERCC spike-in control) in each sample. ERCC sequence analysis showed
241 an average conversion rate of 99.47%, suggesting that bisulfite treatment was efficient (Figure S4E). Due

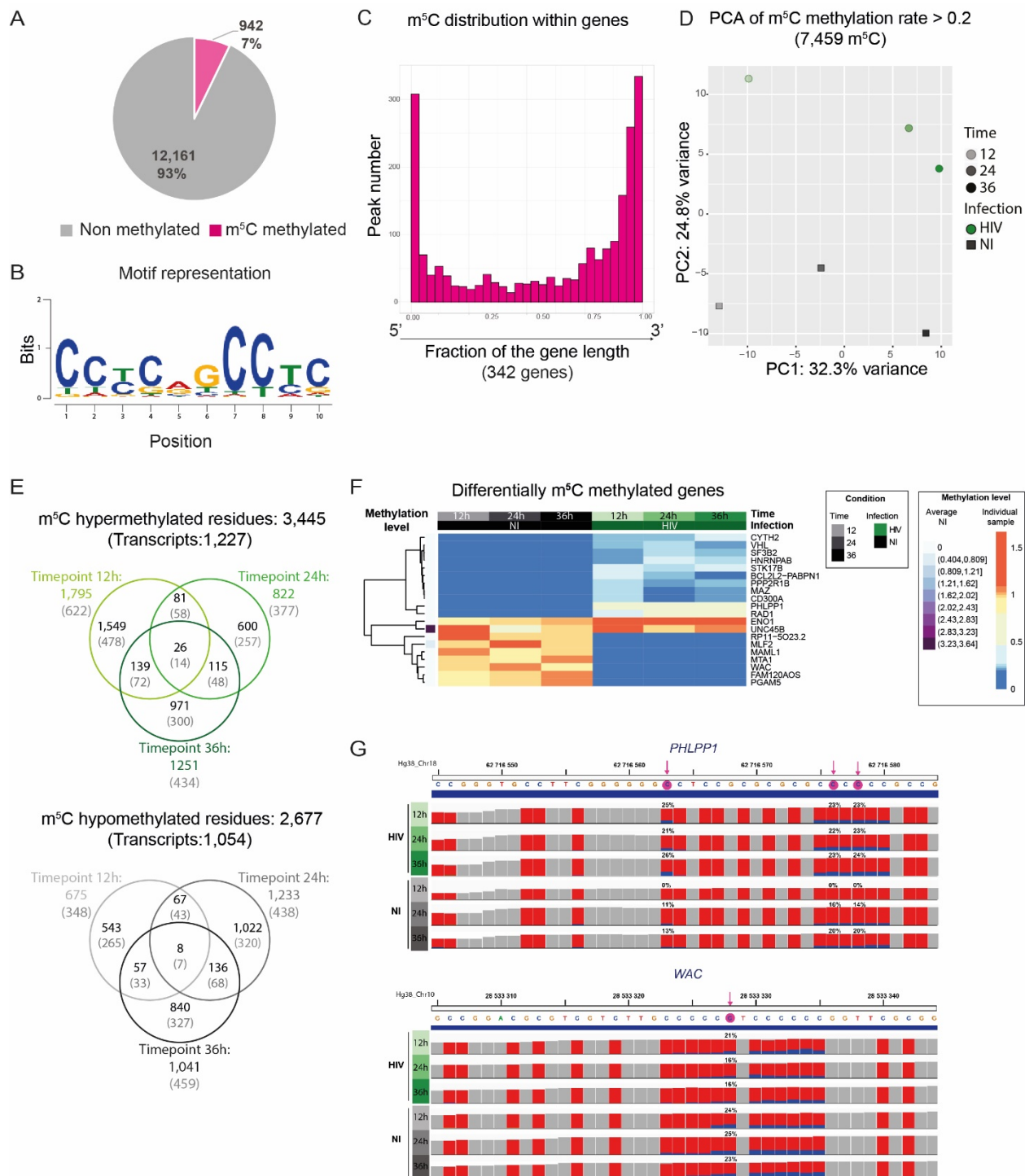
242 the lower quality of bisulfite converted reads with respect to non-converted ones, only transcripts covered
243 with more than 30 reads were retained for further analysis. We could observe different methylation rates
244 among transcripts, hence, to improve the quality of the differential methylation analysis, only cytosines
245 displaying a methylation rate > 20% were used (Table S4). Overall, we identified 2,267 C residues,
246 corresponding to 947 transcripts, present across all the non-infected timepoints with a methylation rate
247 higher than 20% (7% of overall detected transcripts), 567 m⁵C with a methylation rate higher than 50%
248 and 79 with methylation rate >80% (Figure 4A). To date, no consensus was described for m⁵C methylation.
249 We thus analyzed 10 nucleotides surrounding m⁵C residues displaying a methylation rate greater than 80%
250 and we identified a putative consensus sequence in 500 out of 788 highly methylated m⁵C, representing
251 63.4% of total hits (Figure 4B).

252 Consistent with previous studies, m⁵C residues were enriched toward transcript ends and this distribution
253 was not globally affected by HIV infection (Figures 4C and S6) (21).

254 Principal component analysis performed on the totality of m⁵C shows a separation according to time and
255 infection with 32.3% and 24.8% of the variance explained by PC1 and PC2 respectively. This data remained
256 unchanged upon analysis with a more stringent filter for methylated cytosine proportion (conversion rate
257 >50% and conversion rate >80%) (Figure S7). Altogether, our data suggest that HIV affected the m⁵C profile
258 of cellular transcripts. Upon analysis of differentially methylated m⁵C between infected and non-infected
259 cells, we could identify 1,759 hypermethylated m⁵C in infected cells at 12h; 822 at 24h and 1,251 at 36h
260 post infection (corresponding to 622, 377 and 434 hypermethylated transcripts, respectively) (Table S4).
261 Among them 26 m⁵C mapping on 13 different transcripts (and one unidentified transcript) were commonly
262 hypermethylated in infected cells (Figure 4D). We could also identify 675 m⁵C positions hypomethylated in
263 infected cells at 12h; 1,233 at 24h and 1,041 at 36h post infection (corresponding to 348, 438 and 459
264 hypomethylated transcripts respectively) with 8 m⁵C mapping on 7 transcripts commonly hypomethylated
265 upon infection (Figure 4D). The hypermethylated and hypomethylated genes common at the three
266 timepoints are displayed in the heatmap (Table S5 and Figure 4E).

267 Although no statistically significant enrichment was identified by gene ontology analysis, 5 out of the 21
268 genes (23,8%) identified as differentially methylated were already described as interacting with HIV or
269 contributing to its replication.

270



271

272 **Figure 4. HIV infection induces changes in cellular m⁵C profile.** (A) Pie-Chart representing the proportion of m⁵C
 273 methylated transcripts among the totality of detected transcripts (13,103) (B) Identification of a putative consensus
 274 motif for C methylation. Logo representation of the predicted m⁵C motif surrounding C residues displaying a
 275 methylation rate >80%. (C) Histogram plots showing on the x-axis genes
 276 normalized for their length and divided into 30 bins, and for each bin fraction of the gene, the number of
 277 m⁵C residues. Only genes containing a C-T conversion rate >50% were used. (D) PCA of the variance of m⁵C peaks
 278 among all samples. HIV-infected samples (HIV) are shown as green filled circles, non-infected samples (NI) as grey

279 filled squares. Timepoint progression is depicted by the shade of the color. HIV transcripts are not included. **(E)** Venn-
280 Diagrams showing hypermethylated (upper panel) or hypomethylated (lower panel) m⁵C residues upon infection.
281 Values in black represent the number of m⁵C residues, values in grey into brackets represent the number of
282 corresponding transcripts. **(F)** Heatmap of the commonly hyper/hypo methylated transcripts upon infection at the
283 three timepoints. The 21 differentially methylated genes are shown. The average methylation level of the non-
284 infected cells is represented in violet on the left, and was used for normalization. Differential methylation was then
285 normalized to the average methylation intensity of each transcript. **(G)** Examples of a m⁵C hypermethylated (upper
286 panel) and a m⁵C hypomethylated (lower panel) transcript upon infection using IGV viewer. Each C residue in the
287 sequence is indicated as a red bar and the proportion of methylated C is shown in blue (exact proportion values are
288 indicated for the statistically significant residues). The significant methylated C residues are highlighted by a pink
289 arrow in the sequence displayed above the tracks.

290 HIV RNA is both m⁶A and m⁵C methylated

291 Although m⁶A and m⁵C methylation marks were previously reported along HIV RNA molecule, these
292 analyses were performed at a unique time point post-infection and did not consider the putative dynamics
293 of methylation throughout HIV life cycle progression (8-12). We thus took advantage of our temporal
294 design to assess the dynamics of m⁶A and m⁵C epitranscriptomic marks in HIV-infected cells. Furthermore,
295 we compared the methylation profile between intracellular HIV transcripts and vRNA isolated from viral
296 particles.

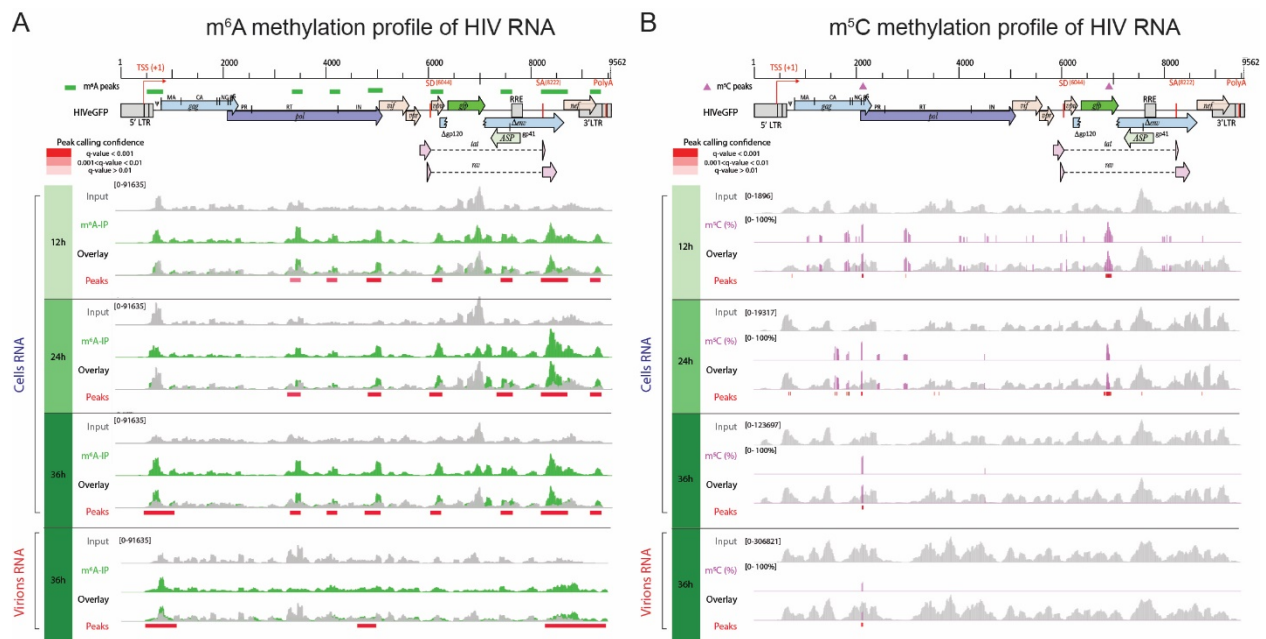
297 Upon m⁶A analysis of intracellular HIV RNA molecules, we identified 7 peaks that were conserved at all
298 timepoints, with enrichment of m⁶A peaks toward the 3' end of the viral sequence (Table S6 and Figure
299 5A). Increased methylation at the 3' region was consistent with previous studies identifying the 3' end as
300 a methylation hotspot and as a binding site for cellular m⁶A readers (9). We also confirmed the presence
301 of two previously reported m⁶A regions in *Pol* (8). However, we identified 2 additional methylated regions,
302 respectively located between *Pol* and *Vif* on one hand, and in *Vpu* on the other hand. Finally, we detected
303 at 36h post-infection a unique peak at the 5' end of the HIV genome, on the packaging signal sequence
304 ψ (ψ), that is also present in the viral particles (Table S7 and FigureS8A).

305 The methylation pattern found on RNA extracted from viral particles is similar to the one present on
306 intracellular HIV transcripts with the exception of the peak found on *Vpu* in close proximity to the splicing
307 donor site.

308 Using a bisulfite conversion approach, we confirmed that cellular HIV RNAs were indeed methylated,
309 however with minimal overlap with methylation hotspots described by Courtney *et al.* (Table S6 and
310 Figure 5B) (12). Upon filtering of low coverage regions and statistical analysis we identified 26 m⁵C at 12h
311 post-infection, 30 m⁵C at 24h post-infection and 7 highly methylated m⁵C residues at 36h post-infection
312 covered by at least 100 reads.

313 Overall, we identified 7 m⁵C residues, common to the 3 timepoints, and clustering all in the vicinity of the
314 HIV *gag-pol* ribosomal frameshift signal with a methylation rate >50%. These highly methylated cytosine
315 are present in viral particles as well as at all timepoints (Figure S8B and Table S7). The mechanism and the
316 role of this time-dependent effect of m⁵C methylation on the HIV RNA sequence needs further
317 investigation.

318



319

320 **Figure 5. HIV RNA is both m⁶A and m⁵C methylated.** Methylation pattern of HIV RNA molecules, isolated from
 321 infected cells over time or from viral particles at 36h post-infection. HIV genome organization is depicted on top of
 322 the panels and methylation marks are indicated as green color rectangles (A) or pink triangles (B) above the genome,
 323 respectively. Detailed read coverage is displayed for each individual sample as tracks below the genome. (A)
 324 Identification of m⁶A peaks on HIV RNA. Input (gray) and m⁶A immunoprecipitated samples (green) are shown.
 325 Putative m⁶A peak calling was performed with MACS2 package after subtraction of the input background (overlay).
 326 Statistically significant peaks are highlighted by a red box, with color shading proportional to the q value (m⁶A peak
 327 track). (B) Identification of m⁵C on HIV RNA. Coverage of HIV genome upon conversion (gray) and detection of m⁵C
 328 (pink) are shown. M⁵C are presented as proportion of converted C. Bar height is proportional to the percentage of
 329 methylated C in the reads covering the position. The track height is set to 100%. M⁵C calling was performed with
 330 MACS2 package. Statistically significant residues are highlighted by a red box, with color shading proportional to the
 331 q value.

332

333 Discussion

334 Epitranscriptomics is a fast growing field of biology which highlighted the role of m⁶A and m⁵C
 335 modifications as specific mRNA marks mostly involved in RNA structural changes and gene expression
 336 regulation. In the present study, we explored (i) the cellular m⁶A- and m⁵C-marked transcriptome
 337 landscape, (ii) the HIV-induced modifications of the cellular epitranscriptome, and (iii) the position of
 338 these specific epitranscriptomic marks on HIV RNA molecule.

339 Using a SupT1 T cell line infected with a VSV-G pseudotyped HIV-based virus, we detected globally 22.5%
 340 transcripts with high confidence (13,103/58,136 genes), among which 15% (1,971/13,103) were
 341 differentially expressed, with 813 genes being upregulated and 1,158 downregulated genes in HIV-
 342 infected cells compared to mock-treated cells. The analysis of the epitranscriptome, with the tools
 343 available today, revealed that 58.9% of genes carried m⁶A methylation (7,724/13,103) (Figure 3B), while

344 m⁵C marks were present on 7% (942/13,103) of transcripts (Figure 4B). These epitranscriptomic marks
345 were mostly enriched towards 3' ends of transcripts, as shown previously, and this distribution was not
346 affected by HIV infection. Furthermore, our data recapitulated the lower abundance of m⁵C methylation
347 compared to m⁶A modification on mRNA molecules (4). In contrast, in presence of HIV, methylation level
348 globally increased and we identified 62 differentially m⁶A-methylated transcripts (59 hypermethylated
349 and 2 hypomethylated) as well as 21 differentially m⁵C-methylated transcripts (14 hypermethylated and
350 7 hypomethylated), common at the three analyzed timepoints. Our data are partially consistent with
351 Tirumuru *et al.*, who observed a 4-7 fold-increase of m⁶A methylation in cells infected with a WT virus,
352 but not upon VSV-G-pseudotyped virus infection, suggesting an Env-mediated signaling increase in
353 methylation (13). The basis of this discrepancy is likely due to differences in the experimental design as
354 Tirumuru *et al.* used a global approach, assessing the level of methylation by m⁶A dot-plot on Jurkat T-cell
355 line, while we used the MeRIP-Seq antibody-based technique on SupT1 cells.

356 Further analysis of the 64 m⁶A-DM transcripts did not reveal any particular enrichment upon gene
357 ontology analysis. Nevertheless, we detected 4 out of 7 GIMAPs in the common list of DM transcripts, and
358 two additional hypermethylated GIMAP members in individual timepoints. GIMAPs are immune-associated
359 proteins displaying a GTPase activity. They have been involved in response to pathogens and have a
360 prominent role in T cell survival and differentiation. The role of GIMAPs in HIV life cycle has never been
361 reported so far and remains to be further characterized.

362 The analysis of the 21 m⁵C-DM transcripts identified a few genes whose products were previously
363 described as interacting with HIV proteins and affecting the viral life cycle. These include Enolase 1 (ENO1),
364 previously described as hampering HIV reverse transcription (22); the splicing factor 3b subunit 2 (SF3B2),
365 shown to interact with Vpr, thereby impairing splicing of some cellular pre-mRNA and impacting Vpr-
366 mediated G₂ cell cycle arrest (23-25); the protein phosphatase 2 scaffold subunit A beta (PPP2R1B),
367 associating with Tat and involved in Tat-mediated apoptosis (26); CD300A, a surface glycoprotein involved
368 in immune response signaling shown to be associated with HIV disease progression markers (27, 28), and
369 shown to be downregulated by Vif (29); and von Hippel Lindau tumor suppressor (VHL), a protein involved
370 in the degradation of hypoxia-inducible-factor and predisposing to cancer when impaired, also known to
371 mediate HIV integrase degradation thereby affecting HIV expression at post-integration steps (30). The
372 role of these methylations on protein expression remains to be investigated, as well as the impact on HIV
373 replication. Nevertheless, these data provide a first roadmap of the impact of HIV on cellular m⁵C-
374 transcriptome.

375 Altogether, these findings suggest that HIV modulates the host methylation profile of the transcriptome

376 and we can thus hypothesize that the modified transcripts are likely to affect the viral life cycle, either
377 promoting it or inhibiting it. Differentially methylated transcripts may thus represent novel HIV-interacting
378 candidate proteins that should be further investigated and characterized.

379 Similar to cellular transcripts, the HIV virion RNA molecule is methylated. We identified 7 m⁶A peaks, that
380 were conserved over time, suggesting a rather stable methylation profile. We observed an enrichment of
381 m⁶A at the 3' of the HIV genome, confirming data from previous studies (8, 9, 11). Our data did not retrieve
382 the two m⁶A peaks previously described to be located in the RRE region, and implicated in enhanced Rev-
383 RRE binding and nuclear export (8). Overall, the studies aiming at investigating m⁶A modifications display
384 minimal overlaps, likely due to protocol differences as mentioned above, and poor resolution of the m⁶A
385 identification approach. Upon comparison between intracellular HIV transcripts and virion RNA we could
386 observe that the m⁶A peak present on *Vpu* and in close proximity of the HIV major 5' splicing donor (SD)
387 was found only in viral transcripts. Maintenance of the SD hairpin secondary structure is essential to
388 ensure correct splicing of viral transcripts by controlling accessibility of the 5' splicing site for the splicing
389 machinery (31). Destabilization of the hairpin loop results in an increase of splicing while its stabilization
390 has the opposite effect. We could speculate that the presence of m⁶A in proximity of the site may induce
391 a change in secondary structure allowing easier access to the splicing machinery, while absence of
392 methylation favors the unspliced HIV RNA form. Moreover, the m⁶A peak present in the 3'UTR region in
393 all intracellular viral transcripts is weak or absent in the viral particle genomic RNA, and could suggest a
394 signal contributing to selective packaging of unmethylated HIV RNA genome (Figure S8).

395 Furthermore, we identified 2 m⁶A peaks, present both on intracellular HIV transcripts and on packaged
396 HIV RNA genome, encompassing the 2 major polypurine tracts (PPT). Although PPT are known for being
397 more resistant to RNaseH-mediated degradation during reverse transcription, the identification of PPT
398 methylation may suggest an additional mechanism providing the observed increased resistance (32).

399 No data were available on m⁵C methylation of HIV transcripts until very recently. Using an
400 immunoprecipitation-based approach to investigate the m⁵C epitranscriptomic mark, Courtney *et al.*
401 identified 18 m⁵C peaks along HIV RNA with an enrichment toward the 3' end of the genome (12). Using
402 a bisulfite conversion (BS-Seq) approach, we confirmed the presence of this modification on intracellular
403 and packaged genomic viral RNAs and identified 7 conserved, highly methylated m⁵C residues, but with
404 only minimal overlap regarding the exact positions of the epitranscriptomic marks. Using a temporal
405 design, we could describe a C cluster at the beginning of *gag* and surrounding the HIV ribosomal frameshift
406 signal that regulates Gag and Gag-Pol precursor protein synthesis. This signal is indeed essential to
407 maintain a tight regulation of the 20:1 Gag/Gag-Pol translation ratio and ensure successful HIV replication

408 (33). The identification of an m⁵C hotspot close to the frameshift signal may thus point to an additional
409 mechanism involved in the post-transcriptional regulation of Gag and Gag-Pol production.

410 Although m⁶A and m⁵C methylations are considered as the most abundant modifications on mRNA
411 molecules, additional epitranscriptomic marks may be present and impact HIV-host interactions, such as
412 2'-O-methylations (12, 34). Indeed, Ringear *et al.* recently showed that HIV transcripts can be methylated
413 at the 2' hydroxyl of ribose, hence 2'-O-methylation, via a specific methyltransferase, FTSJ3, specifically
414 recruited by TAR-RNA binding protein (TRBP) (34). They identified 17 A or U residues containing this
415 specific methylation on the viral RNAs. They demonstrated that 2'-O-methylations were important for
416 viral transcripts to be recognized as endogenous RNA mimics and thus escape innate immune sensing and
417 degradation. Differential analysis of 2'-O-methylation marks upon HIV infection may provide additional
418 insights in HIV life cycle (12, 34).

419 Overall, this study provided an overview of m⁶A and m⁵C modifications on both viral and cellular
420 transcriptomes over time, identifying the dynamic impact of HIV infection on cellular RNA modifications,
421 and identifying novel candidates as putative factors involved in HIV replication. Further investigation of
422 these candidates, using overexpression or knock-out assays, may reveal a role as HIV dependency factor
423 or inhibitory factor.

424 The existence of RNA modifications and their potential modulation by HIV proteins offer a new layer of
425 opportunities to hijack the host cellular machinery to promote viral replication and evade the innate
426 immune response. Therefore, identifying all types of differentially methylated or modified transcripts
427 upon HIV infection may lead to the uncovering of novel host factors involved the HIV-host interplay.

428 **Methods**

429 **Cells and plasmids**

430 Human Embryonic Kidney 293T (HEK293T) cells were cultured in D10 (Dulbecco's modified Eagle medium
431 (DMEM) containing 1x glutamax (#61965-026, Invitrogen), supplemented with 10% heat-inactivated Fetal
432 Bovine Serum (FBS) and 50 µg/ml Gentamicin) and maintained at a maximal confluence of 80%.

433 SupT1 cells are human T cell lymphoblasts. They were cultured in R10 (RPMI 1640 with 1x glutamax
434 (#61870-010, Invitrogen) containing 10% heat-inactivated FBS and 25 µg/ml Gentamicin) and split twice
435 a week at 0.5x10⁶ cells/ml to maintain a maximal concentration of 1x10⁶ cells/ml.

436 The following DNA constructs were used in this study: For viral infection, we used pNL4-3ΔEnv-GFP (NIH
437 AIDS Research and Reference Reagent program, Cat. #11100) that encodes the HIV vector segment with

438 a 903 bp deletion in the *env* ORF in which the *gfp* ORF was introduced. For pseudotyping, the plasmid
439 pMD.G coding for the vesicular stomatitis virus G envelope (VSV-G) was used (35).

440

441 **HIV production and infection**

442 For production of HIV-based vector NL4-3-ΔEnv-GFP/VSV-G (named hereafter HIV-eGFP), 2.5 million of
443 HEK293T cells were seeded in 10 cm dishes and incubated over night at 37°C/5% CO₂. The next day, cells
444 reached about 60 % confluence and were transfected with a total of 10 μg of DNA, *i.e.* 7.5 μg of pNL4-3-
445 ΔEnv-GFP and 2.5 μg pMD2.G coding for the VSV-G envelope, using the jetPRIME kit (Polyplus
446 transfection) and according to manufacturer's instructions. Briefly, DNA was diluted into 500μl of supplied
447 buffer, mixed with 30μl of jetPRIME reagent and incubated 10 minutes at room temperature. Transfection
448 mixture was then added to the cell dropwise. Fifteen hours after transfection, cells were washed once
449 with D10 and incubated for 33h in 293SFM medium (#11686029, Thermo Fisher Scientific). HIV-GFP
450 particles were harvested 48h after transfection, filtered through 0.45 μm and concentrated on Centricon
451 units (Centricon Plus-70/100K, Millipore). Viral titers were measured by HIV p24 Enzyme-linked
452 immunosorbent assay (ELISA) kit (Innogenetics).

453 SupT1 cells (5×10⁶ cells) were either mock-treated or infected with 5 μg p24 equivalent of HIV-GFP by
454 spinoculation at 1500 g for 30 min at 20°C, in presence of 4 μg/ml polybrene (Sigma), in 400 μl final volume
455 in 14 ml round bottom polypropylene tubes - a total of 50 tubes were used for mock condition and 50
456 tubes for infected condition to obtain a total of 250 million cells for each condition. Cells were then
457 pooled, washed three times with culture medium, resuspended at 10⁶ cells/ml in R-10 and further
458 incubated in T75 flasks (8x31ml).

459 At 12, 24 and 36 hours post-infection, cellular samples (~50×10⁶ cells in 50 ml) were collected for viral
460 and cellular measurements. Briefly, 0.5 ml of the cell cultures were used for cell counting and viability
461 assessment by trypan blue exclusion, using a ViCell Coulter Counter (Beckman Coulter). Remaining cells
462 were centrifuged at 300 g for 10 min. Viral supernatant was collected: 950 μl were mixed with 50 μl NP-
463 40 (0,5%) and stored at -80°C until particle concentration assessment by p24 ELISA (Innogenetics) while
464 the rest of the supernatant was concentrated by filtration on Centricon units (Centricon Plus-70/100K,
465 Millipore) and frozen at -80°C for RNA extraction. Cells were washed with R10 once, centrifuged again,
466 resuspended in 5 ml R10 (~10⁷ cells/ml) and separated as follows: (i) 50 μl of cell suspension were
467 resuspended in Cell Fix 1× (Becton Dickinson) for assessment of GFP expression and infection success by
468 FACS analysis (Accuri C6 FACS, Becton Dickinson), (ii) aliquots of 1 ml of cell suspension (~10⁷ cells) were

469 centrifuged, resuspended in 1ml of Trizol reagent (#15596026, Invitrogen) and stored at -80°C for further
470 RNA extraction and transcriptome analyses.

471

472 **RNA extraction**

473 Total RNA was extracted from both concentrated viral particles and cells using Trizol Reagent (#15596026
474 Invitrogen) according to suppliers's instructions. Briefly, samples were thawed at room temperature and
475 200µl chloroform were added to the mixture. Samples were centrifuged for 30min at 10.000g, at 4°C and
476 the RNA-containing, aqueous (upper) phase was transferred to a fresh tube and subjected to precipitation
477 with 0,5 ml of isopropanol for 1h at -80°C. Samples were then centrifuged for 10 min at 12000g, washed
478 once in 1ml of 75% ethanol and resuspended in 50 µl H₂O.

479 For poly(A) RNA purification, 200µl Dynabeads Oligo(dT)₂₅ (#61005, Life Technologies) were washed twice
480 with 1ml of binding buffer (20 mM Tris-HCl, pH 7.5, 1.0 M LiCl, 2 mM EDTA) and incubated with aliquots
481 of 75 µg RNA in 100µl final volume for 15 minutes at room temperature on a wheel. Samples were then
482 washed twice with 500µl washing buffer (10 mM Tris-HCl, pH 7.5 ,0.15 M LiCl, 1 mM EDTA 10 mM Tris-
483 HCl, pH 7.5), and subjected to a second incubation with the same RNA sample. Poly(A) selected mRNA
484 was recovered through elution by a 2 min incubation with 20µl Tris-HCl (10mM) at 80°C. PolyA depleted
485 RNA from the 36h NI samples was purified and kept as a spike-in control for bisulfite conversion
486 experiments. RNA was purified and concentrated using a column-based kit (#RNA1013, Zymo Research),
487 fragmented during 15 min at 70°C using Ambion RNA Fragmentation Reagents (#AM8740, Life
488 Technologies), in order to obtain fragment of 100-200nt and purified again as above. An aliquot of
489 fragmented RNA (100 ng) was retained as a control for RNA sequencing (input) while the rest was used
490 for MeRIP-Seq and bisulfite conversion allowing m⁶A and m⁵C analysis respectively. At every step, integrity
491 and peak size of the RNA was assessed on a Fragment Analyser (AATI #DNF-472).

492

493 **m⁶A-modified RNA immunoprecipitation sequencing (MeRIP-Seq)**

494 For MeRIP (#17-10499, Millipore), 5 µg of fragmented mRNA was incubated with 5 µg of anti-m⁶A antibody
495 or anti-IgG antibody (negative control) previously coupled with 25 µl of A/G-coated magnetic beads in 500
496 µl IP Buffer for 2h at 4°C following manufacturer's recommendations. Samples were placed on a magnetic
497 stand for 5 minutes and the unbound RNA was discarded. The beads were then washed three times with
498 500µl IP buffer and bound RNA was released by two rounds of elution of 1 hour each with 20mM of free
499 m⁶A peptides (7mM N⁶-Methyladenosine.5'-monophosphate sodium salt). RNA was purified and
500 concentrated in 20µl of water, using a column-based kit (# RNA 1013, Zymo Research). We recovered

501 normally between 15 and 25ng of associated RNA from samples immunoprecipitated with a specific anti-
502 m⁶A antibody. Libraries for sequencing (input RNA-Seq and MeRIP-Seq) were prepared using Illumina
503 TruSeq Stranded mRNA kits (#20020594, Illumina), starting the protocol at the Elute-Prime-Fragment
504 step, and with a protocol modification consisting in incubating the samples at 80 °C for 2 minutes to only
505 prime but not further fragment the samples. Samples were sequenced on a HiSeq 2500 Illumina on 4
506 lanes, using single end reads of 125nt (Genomic Technology Facility (GTF), University of Lausanne).
507 RNA-Seq data were aligned to a combined hg38 (chr 1-22, X, Y) and HIV genome FASTA using the STAR
508 aligner, and keeping only uniquely mapping reads. Data were analyzed in collaboration with the Swiss
509 Institute of Bioinformatics (SIB) and the Genomic Technology Facility (GTF), University of Lausanne.

510

511 **RNA bisulfite conversion sequencing (BS-Seq)**

512 Bisulfite treatment was performed using the EZ RNA methylation Kit (#R5001, Zymo Research). Briefly,
513 500 ng of poly(A)-selected RNA were spiked-in with 500pg of polyA-depleted RNA (to ensure rRNA
514 representation) as a control for bisulfite conversion. mRNA was mixed with 130µl of RNA conversion
515 solution and converted using three cycles of 10 min denaturation at 70°C followed by 45 min at 64°C in a
516 final volume of 200 µl. After conversion, mRNA was bound to a RNA purification column and desulfonated
517 by addition of 200µl RNA Desulfonation Buffer during 30 minutes at room temperature. Purification was
518 performed using the kit according to manufacturer's recommendations. RNA quantity and quality was
519 determined by analysis on a Fragment analyser (AATI) using the High sensitivity RNA kit (#DNF-472, AATI).
520 The efficiency of bisulfite treatment was tested by RT-PCR-mediated bisulfite analysis of spiked-in rRNA
521 (C4447 in 28S rRNA is 100% methylated). Briefly, 4µl of bisulfite converted RNA were subjected to RT with
522 High Capacity cDNA reverse transcription kit (Applied Biosystems #4368814) according to manufacturer
523 procedure and incubated with the following program: 25°C – 10 min; 37°C – 120 min; 85°C 5 min. PCR was
524 performed on 6µl of cDNA using the AccuPrime™ Pfx SuperMix (Thermo Fisher Scientific # 12344-040)
525 with primers annealing on the 28S ribosomal RNA (primerH28SF, H28SR table1). PCR products were
526 sequenced by Next Generation Sequencing, and resulting sequences aligned to the Human 28S. Cytosine
527 in position 4447 was used as control of non-converted cytosine, while surrounding cytosines were used
528 as a control of C-T conversion.

529 Libraries for sequencing were prepared using the Illumina TruSeq Stranded mRNA kit as described above
530 (*i.e.* entering the protocol at the Elute-Prime-Fragment step and with the modification) and sequenced on
531 two lanes of Illumina HiSeq 2500 as described above.

532

533 **FACS analysis**

534 FACS analysis of infected cells was performed on a BD Accuri C6 machine. About 2×10^5 cells were washed
535 twice in Robosep buffer (#20104, Stemcell Technologies) and fixed in 300 μ l CellFix buffer 1X (#340181,
536 BD) for at least 3h at 4°C. The GFP was then monitored by FACS in the FL-1 channel to monitor infection
537 success. Analysis was carried out using FlowJo software.

538

539 **Bioinformatic analyses**

540 The analyses described in this section apply to both intracellular transcripts (host mRNAs and vRNAs) and
541 virion-incorporated RNA data.

542 **m⁶A and gene expression quantification**

543 The m⁶A modification and input libraries underwent a first quality check with FASTQC
544 [<http://www.bioinformatics.babraham.ac.uk/projects/fastqc/>]. FASTQ files were trimmed with Atropos
545 (36). The following adapter sequences - AGATCGGAAGAG, CTCTCCGATCT, AACACTCTTCCCT,
546 AGATCGGAAGAGCG, AGGGAAAGAGTGTT, CGCTCTCCGATCT - were removed after trimming of low-
547 quality ends (a Phred quality cutoff of 5 has been applied) as specified by the manufacturer
548 ([https://support.illumina.com/downloads/illumina-adapter-sequences-document-](https://support.illumina.com/downloads/illumina-adapter-sequences-document-1000000002694.html)
549 [1000000002694.html](https://support.illumina.com/downloads/illumina-adapter-sequences-document-1000000002694.html)). Only reads with a minimum length of 25 base pairs after trimming were retained.
550 Trimmed reads were aligned to an assembly of the Hg38 human genome and HIV [Integrated linear pNL4-
551 3 Δ Env-GFP] genome. The software used for the alignment was HISAT2 (37). Aligned reads were indexed
552 and sorted with SAMtools (38).

553 Post-alignment quality of the reads was performed with SAMtools stat and Qualimap 2 (39). Quality
554 measures have been collected and summarized with multiQC (40).

555 HIV genome has homologous 634 bp sequences in the 5' LTR and 3' LTR. Multimapping reads from 5' LTR
556 have been realigned to the corresponding 3' LTR region with SAMtools.

557 Abundance quantification of transcripts on input libraries has been performed with Salmon (41). HIV
558 expression level has been quantified by directly counting reads mapping to the viral genome.

559 m⁶A peaks were identified with the peak calling software MACS2 (v 2.1.2)(42). Caution was applied in the
560 choice of MACS2 running parameters, to allow the tool to correctly work on RNAseq data. In RNA-Seq data
561 the peak calling can be affected by the gene expression level, and short exons may potentially be miscalled
562 as peaks. Hence, signal from input must be subtracted from m⁶A signal, without the the smoothing
563 routinely applied by MACS2 to DNA based data.

564 'callpeak' sub-command from MACS2 was run with the following parameters: `-keep-dup auto` (controls
565 the MACS2 behavior towards duplicate reads, 'auto' allows MACS to calculate the maximum number of

566 reads at the exact same location based on binomial distribution using $1e-5$ as p-value cutoff), -g 2.7e9
567 (size of human genome in bp), -q 0.01 (minimum FDR cutoff to call significant peaks), --nomodel (to bypass
568 building the shifting model, which is tailored for ChIP-Seq experiments), --slocal 0 --llocal 0 (setting these
569 2 parameters to 0 allows MACS2 to directly subtract, without smoothing, the input reads from the m⁶A
570 reads), --extsize 100 (average length of fragments in bp), -B -SPMR (to generate library size normalized
571 bedGraph track for visualization).

572 In order to compare infected vs non-infected samples, the differential peak calling sub-command of
573 MACS2, 'bdgdiff', was used. 'bdgdiff' takes as inputs the bedGraph files generated by 'callpeak'. First, we
574 run 'callpeak' with the same parameters as above, but without the -SPMR option (output unnormalized
575 tracks), which is not compatible with 'bdgdiff'. Then, for each time point we run the comparison of
576 infected versus non-infected samples with 'bdgdiff', subtracting the respective input signal from the m⁶A
577 signal and providing the additional parameters -g 60 -l 120.

578

579 **Bisulfite conversion analyses**

580 Cutadapt (43) was applied for read trimming, using parameters of --minimum-length=25 and the adapter
581 "AGATCGGAAGAGCACACGTCTGAAC". Trimmed reads were subsequently reverse complemented using
582 seqkit (44).

583 Quality control was performed by employing FastQC to examine samples for (a) poor read quality, and (b)
584 contamination of which there was no supporting evidence.

585 The application meRanGh from the meRanTK package (20) was leveraged to make an index file for
586 alignment consisting of the hg38 reference genome supplemented with the HIV genome. Aligning again
587 employed meRanGh with parameters enabling unmapped reads (-UN), multi-mapped reads (-MM) to be
588 written to output files. Additionally, the output bedGraph (-bg) was produced.

589 Reported Regions were filtered by those with at least a 10 read coverage (-mbgc 10). To account for HIV
590 LTR regions being multi-mapped, and not thus not being present in the alignment output file, Sambamba
591 (45) merge was employed to filter reads in the HIV genome upstream of the 8500bp locus and append
592 them to the final alignment.

593 FeatureCounts (46) was employed at the exon and CDS level for the hg38 and HIV genomes, respectively.
594 Methylation calling was completed via the meRanCall tool, provided by meRanTK, with a read length (-rl)
595 parameter of 126, an error interval of .1 used for the methylation rate p-value calculation (-ei), an
596 expected conversion rate of .99 (-cr). MeRanCompare was employed with a significance value of .01 as
597 the minimal threshold for reporting. For its size factors parameter, MeRanTK's included utility

598 estimateSizeFactors.pl was employed on each of the time points, and produced values of (.8102, 1.2342),
599 (1.1894,.8408), (0.6562,1.5240) for (not infected, infected) across time points 12, 24, and 36h
600 respectively.

601

602 **Differential Gene Expression (DGE) analysis**

603 Transcript abundance and counts estimated by Salmon for the input samples were imported into an R
604 session (version 3.5.1) using the package tximport (47). The same package was used to summarize
605 transcript level expression at the gene level.

606 Low count genes have been removed with the method 'filtered.data' from the package NOISeq (48).
607 'filtered.data' method 1 removes those genes that have an average expression per condition less than 3
608 CPM (Counts Per Millions) and a coefficient of variation per condition higher than cv.cutoff = 100 (in
609 percentage) in all the conditions.

610 The filtered gene table was the processed with the package for differential gene expression analysis (49).
611 First, exploratory PCA plots were generated with the PCA plot function on counts transformed with the
612 rlog method in DESeq2. Then, differential expressed genes were called with an adjusted (Benjamini-
613 Hochberg method) p-value threshold of 0.01. To take into account the effect of cell culture time together
614 with that of HIV infection, we asked DESeq2 to fit a Generalized Linear Model (GLM) which included both
615 effects: design = ~ infection + time. Two lists of differentially expressed (DE) genes according to infection
616 and time were thus obtained. To further separate the effect of the HIV infection from the time one, we
617 produced a list of 'HIV only' DE genes, by removing from the list of infection related DE genes those in
618 common with the list of time-related DE genes.

619 A PCA plot with this 'HIV only' DE gene list was produced in order to highlight the effect of HIV infection,
620 and heatmaps with the gene expression level of these genes were also drawn.

621

622 **m⁶A differential peak calling analysis**

623 MACS2 'callpeak' generated a list of peaks for each time point and each infection status (infected and
624 non-infected). MACS2 "bdgdiff" generated 3 lists (common peaks, up and down regulated upon HIV
625 infection) for each time point comparison. These lists of peaks were further processed and analyzed with
626 the R package diffbind (50), and annotation with overlapping genes was provided by the package
627 ChIPpeakAnno (51).

628 To reduce the number of false positives, only the peaks called by both MACS2 methods ('callpeak' and
629 'bdgdiff') were retained in the following analyses. For purpose, for each time point and infection status,

630 we intersected the list produced by 'callpeak' with the corresponding lists produced by 'bdgdiff' (the
631 common peaks and condition specific peaks). We thus obtained a high confidence peak list for each time
632 point and condition.

633 We defined a measure for peak intensity based on the number of reads overlapping with each peak. For
634 counting the overlapping reads, the function dba.count from DiffBind was used. First, we created a
635 consensus peak set with the union of the high confidence peak lists. Reads overlapping with a span of 100
636 bp around the summit of the peaks in the consensus were counted, normalization factors were computed
637 using edgeR TMM method (52), and the reads in the m⁶a input were subtracted to separate methylation
638 from expression level effects. The normalized counts at each peak, which we will call peak scores, were
639 used to generate the PCA plot, the peak distribution along gene length, and heatmaps.

640 The presence of the m⁶A binding motif ("DRACH") was assessed using the function scan_sequences from
641 the package "universalmotif" (53) over the consensus list of peaks.

642 An unsupervised motif search was also performed. From the consensus peak set, we extracted the
643 nucleotide sequence (from the reference genome Hg38) of an interval of 10bp upstream and 10bp
644 downstream from the center of each peak. The list of 17657 sequences was used as input for the tool
645 DREME (54), from MEME suite (5.1.0)(55), which performed the motif discovery.

646 Peak distributions along genes were computed by dividing each gene in 30 intervals and adding up the
647 scores of peaks belonging to each interval for all genes (in other words, computing the sum of the peaks
648 in each interval weighed by the scores). The distributions were plotted at each time point and condition.

649 In order to compare the modification of m⁶A RNA methylation specific to HIV infection, we intersected
650 the up (down) regulated peak lists of all 3 time points, and, for late infection response, at 24h and 36h
651 time point only. We summarized these results at the gene level (obtaining a 'gene methylation score'), by
652 adding up the scores of the peaks in each gene. The methylation score of up and down methylated genes
653 upon HIV infection were plotted as heatmaps.

654

655 **m⁵C differential methylation calling analysis**

656 The m⁵C data analysis follows the line of the m⁶A one described above. The lists of methylated C generated
657 by meRanCall tool were further processed and analyzed with the R package DiffBind and annotation for
658 overlapping genes was provided by the package ChIPpeakAnno.

659 In order to reduce the number of false positives in m⁵C called bases, beside the adjusted p-value threshold
660 of 0.01 applied by meRanCall, we introduced an extra threshold on coverage, asking that the retained m⁵C

661 bases having at least 30 read coverage. This number was adjusted by the total number of reads in each
662 library to have an even filter across samples.

663 Furthermore, a consensus set of m⁵C sites was created by the union of the m⁵C called bases from all
664 samples, asking that a methylated site appears in at least 2 samples. The methylation rate (number of
665 methylated C over total number of C) at each base was used as methylation intensity score to generate
666 the PCA plot, the m⁵C distribution along gene length, and heatmaps.

667 A motif discovery was performed with MEME (5.1.0)(55). A list of 788 sequences of 10 bp surrounding
668 both sides of methylated bases was input to MEME. This list is a high confidence list of methylated sites
669 made by joining (union) the bases with a methylation rate greater than 0.8 from all samples.

670 m⁵C distributions along genes were computed by dividing each gene in 30 intervals and adding up the
671 methylation rate of m⁵C belonging to each interval for all genes (in other words, computing the sum of
672 the m⁵C sites in each interval weighed by the methylation rate). The distributions were plotted at each
673 time point and condition.

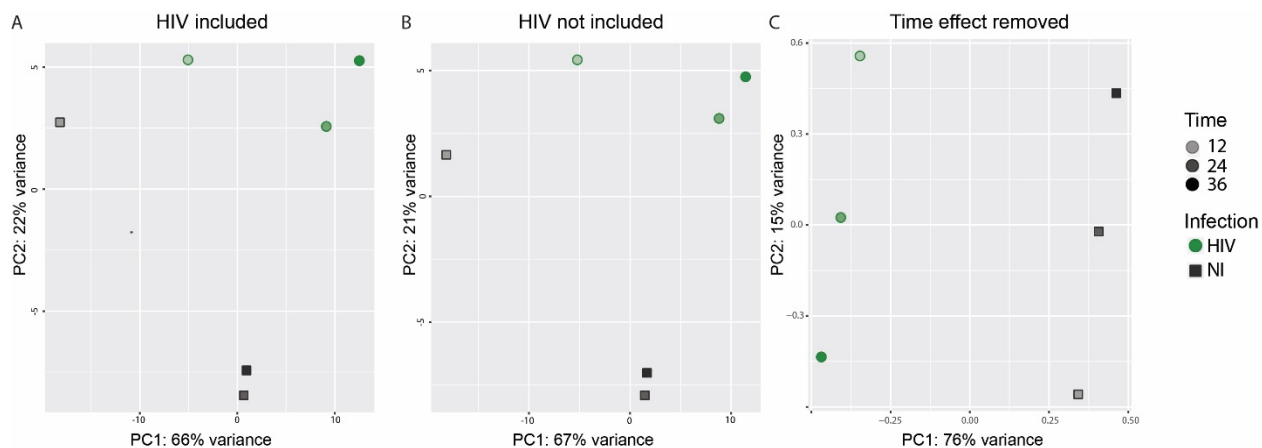
674 In order to compare the modification of m⁵C RNA methylation specific to HIV infection, we intersected
675 the up (down) regulated peak lists of all 3 time points, and, for late infection response, at 24h and 36h
676 time point only. We summarized these results at the gene level (obtaining a 'gene methylation score'), by
677 adding up the methylation rates of the bases in each gene. The methylation scores of up and down
678 methylated genes upon HIV infection were plotted as heatmaps.

679

680 **Supplementary Figures and Data**

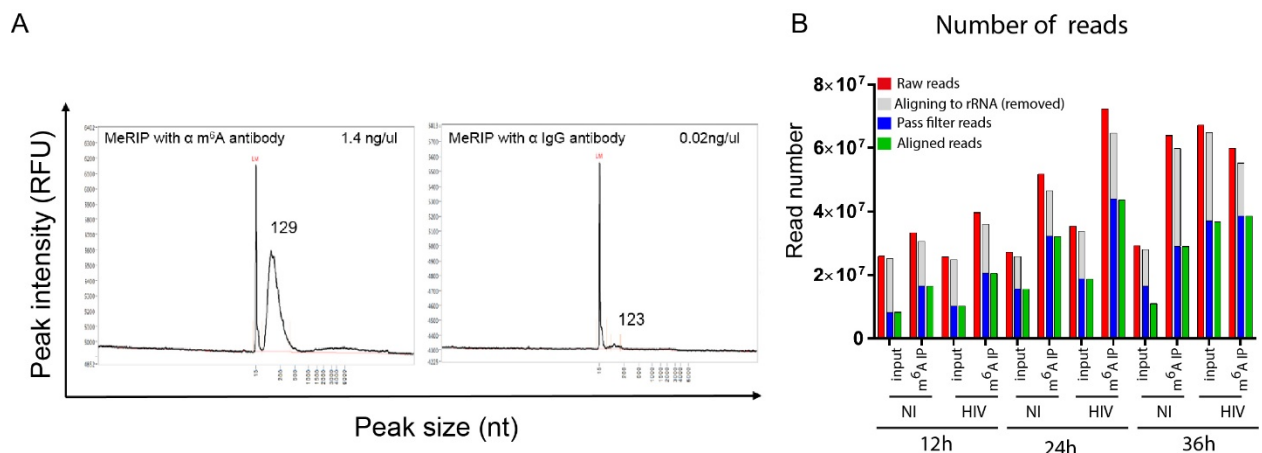
681 **Supplementary Figures**

682



683

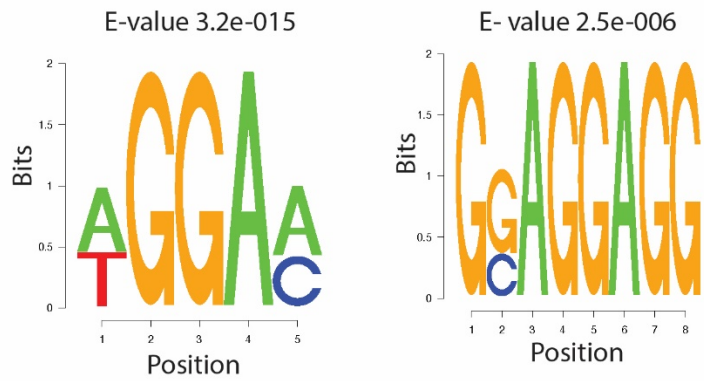
684 **Figure S1: Time and HIV infection effects on gene expression.** Principal component analysis (PCA)
 685 representing gene expression variation across samples, in presence (A) or absence (B) of HIV transcripts
 686 and upon removal of time effect (C). HIV-infected samples (HIV) are represented as green filled circles,
 687 non-infected samples (NI) as grey filled squares. Increasing timepoints (12h, 24h, 36h) are depicted by
 688 increasing color shading.



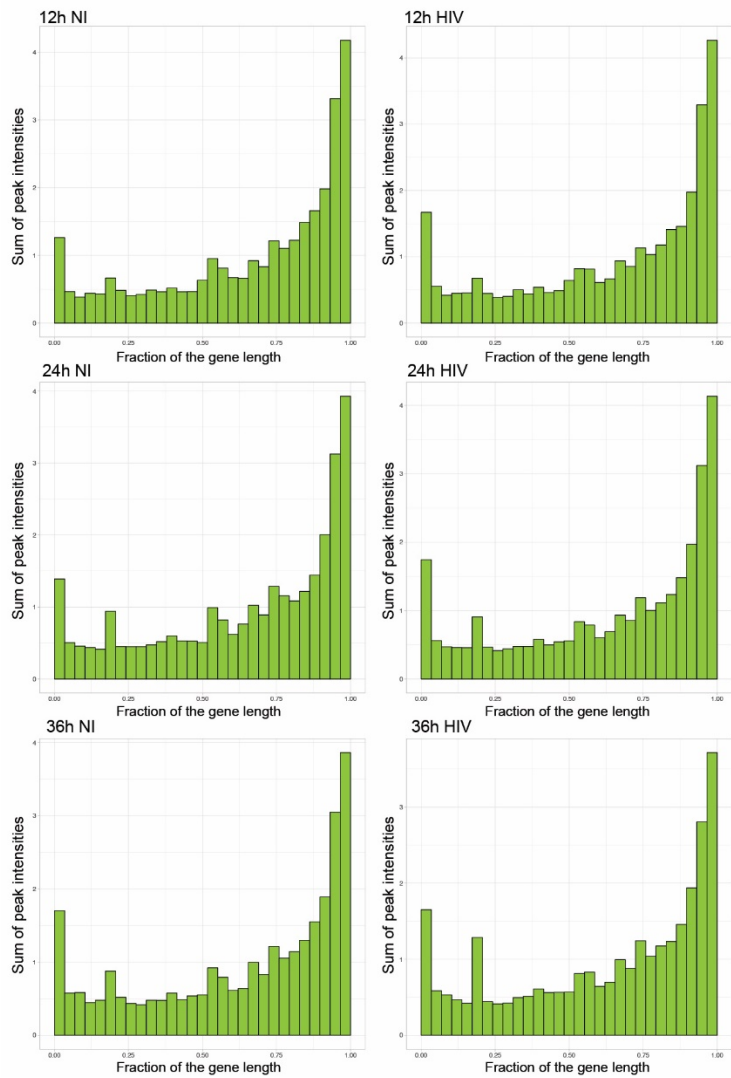
689

690 **Figure S2. M⁶A quality controls.** (A) Representative Fragment Analyzer outcome assessing the size and
 691 the quantity of RNA fragments recovered after MeRIP-Seq with a specific anti-m⁶A antibody (left) and with
 692 the non-specific anti-IgG antibody (right). The x-axis represents the nucleotide size of the peak, while the
 693 y-axis quantifies the intensity of the peak in Relative Fluorescence Units (RFU). LM: low marker reference.
 694 (B) **Sequencing read analysis.** Amount of raw reads (red), reads aligning to rRNA (grey), clean pass filter
 695 reads (blue) and aligned reads (green) retrieved for input and m⁶A-immunoprecipitated (IP) samples. HIV:
 696 HIV-infected samples; NI: non-infected mock samples.

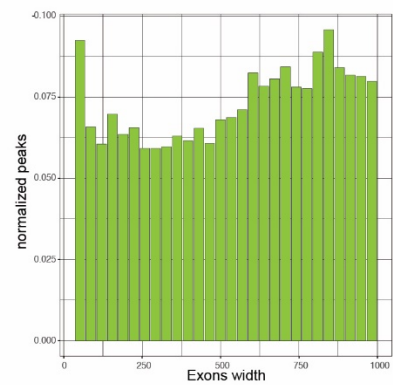
A m⁶A motif representation



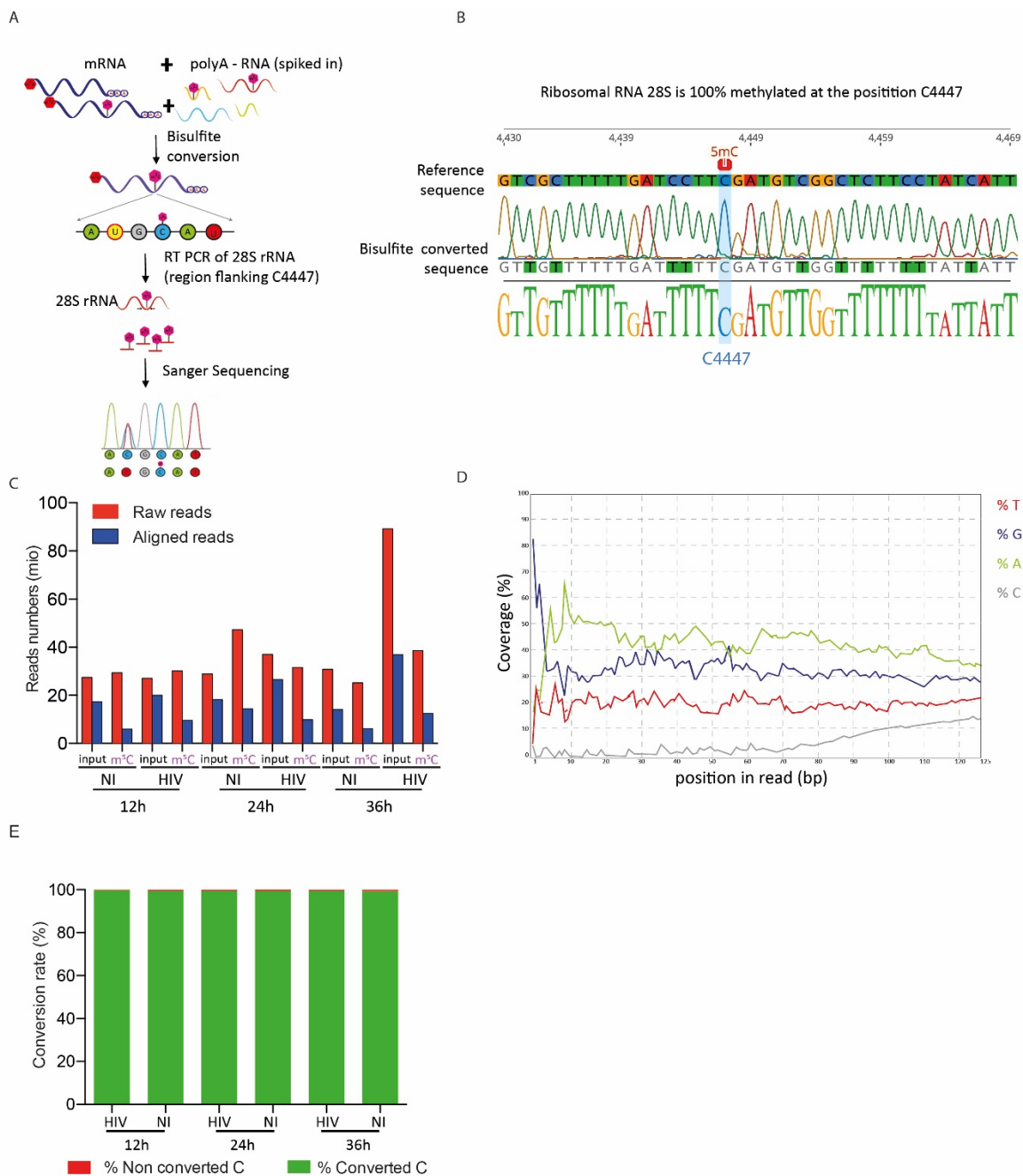
B m⁶A peak distribution within genes



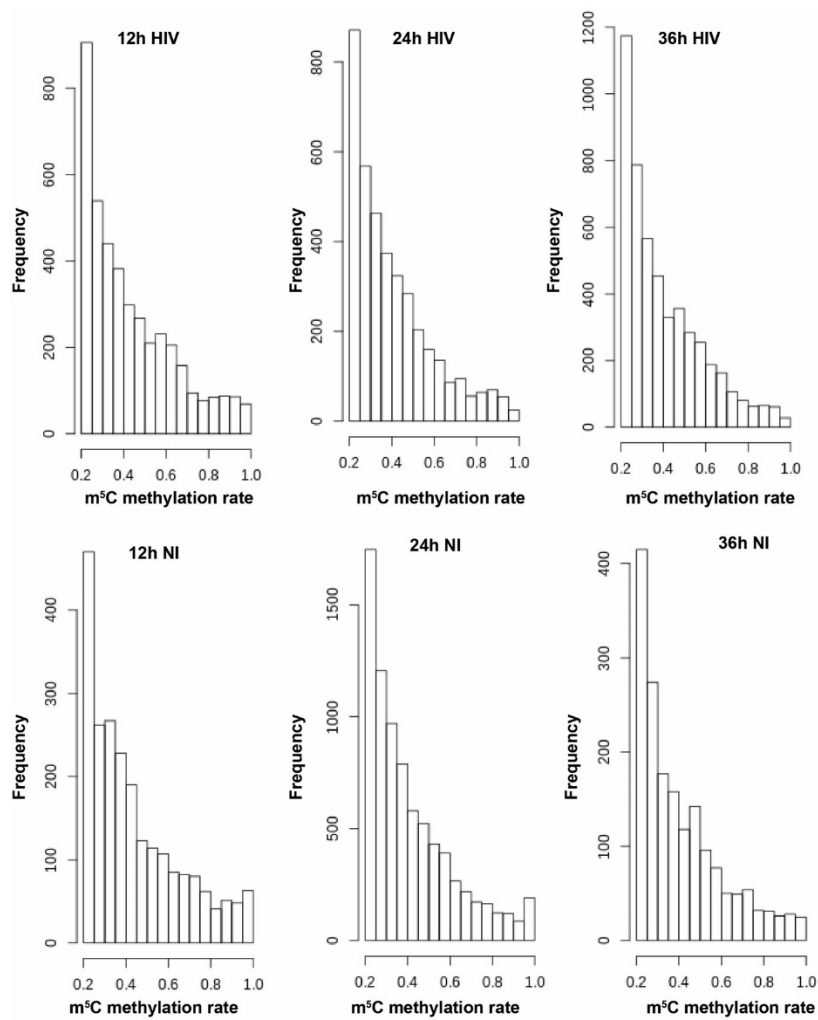
C m⁶A peak distribution within exons



700 **Figure S3. m⁶A peak distribution. (A)** Representation of the two most enriched m⁶A motif in our dataset
 701 **(B)** Frequency of m⁶A methylation along the gene in each sample. Histogram plots showing on the x-axis
 702 genes normalized for their length and divided into 30 bins, and for each bin fraction of the gene, the
 703 number of m⁶A peaks weighted for the peak intensity (peak surface) was assessed. **(C)** Frequency of m⁶A
 704 peak distribution according to exon width. Exons were binned according to their width (x-axis). The
 705 number of m⁶A peaks (y-axis) per binned exon width was normalized by the exon width.



707 **Figure S4. M⁵C quality controls. (A)** Schematic representation of the evaluation of bisulfite conversion
708 efficiency by qPCR. The 100% methylated C4447 of the 28S human rRNA was used as a positive control to
709 evaluate the efficacy of bisulfite conversion treatment. Purified mRNA was spiked-in with polyA-depleted
710 RNA, to ensure rRNA representation, and exposed to bisulfite treatment, triggering C to U conversion in
711 absence of methylation while methylated C (pink hexagone mark) were protected and unmodified. A
712 fraction of the bisulfite converted RNA was subjected to RT-PCR in order to amplify a 200 bp region of the
713 28SrRNA flanking C4447 for Sanger sequencing. **(B)** Electropherogram of a representative sequence
714 retrieved after RT-qPCR. The blue arrow highlights the conserved methylated C residue at position 4447,
715 identified as a C upon sequencing (top panel). In contrast, non-methylated C residues (blue in the
716 reference sequence on the bottom panel) are converted to T (green nucleotides, as shown on the top
717 panel) upon bisulfite treatment, RT and sequencing. **(C)** Amount of raw reads (red) and clean pass filter
718 reads (blue) retrieved for the bisulfite converted samples. HIV: HIV-infected samples; NI: non-infected
719 mock samples. **(D)** Representation of the read per base content along every position of the read. On the
720 x-axis is depicted the position in the read, on the y-axis the total coverage proportion of each base. **(E)**
721 Conversion rate assessment. Non-methylated ERCC control sequences were spiked in each sample to
722 assess the conversion rate. Percentage of successfully converted C are represented in green, non-
723 converted C are represented in red. The average conversion rate across samples was 99.47%.

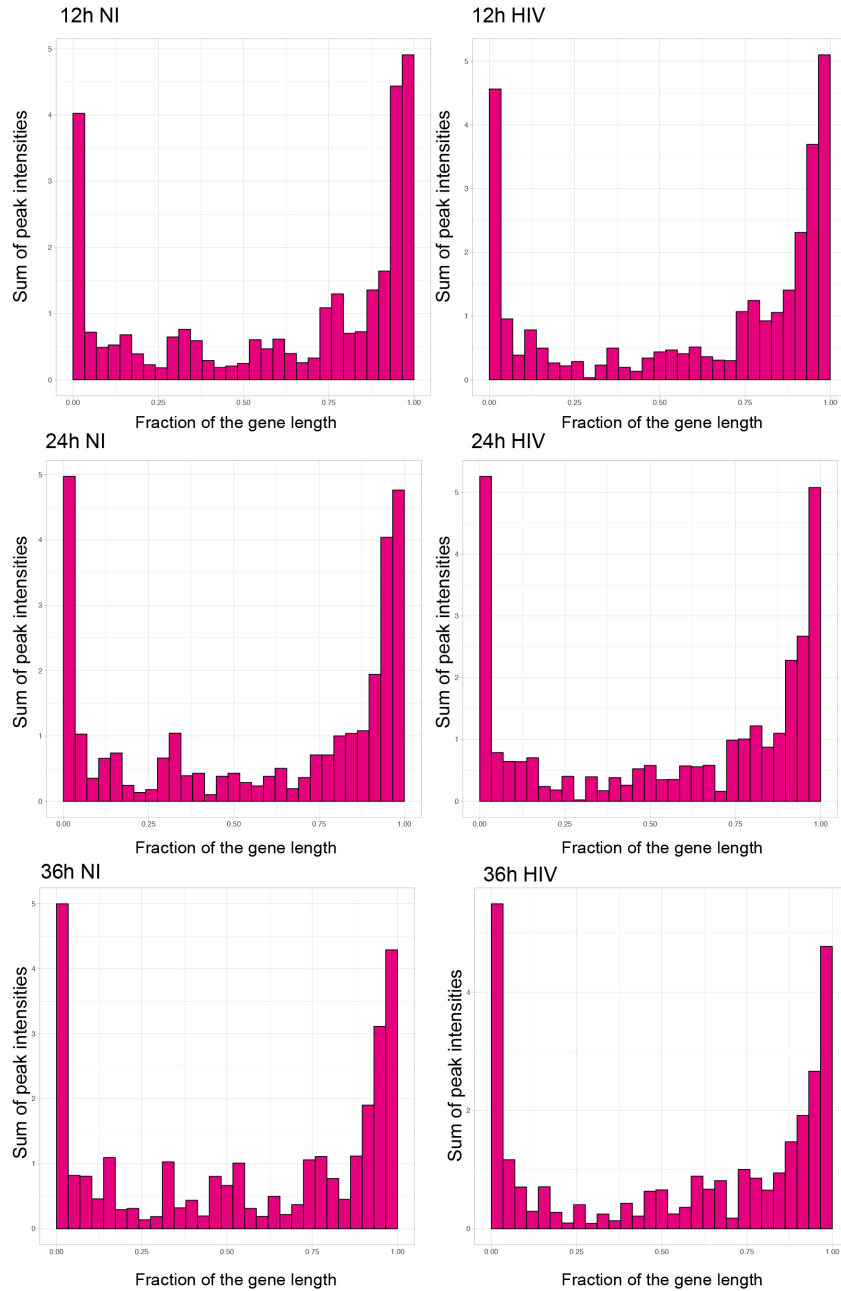


724

725 **Figure S5. Frequency of m⁵C methylation.** Histogram samples showing the number of C residues (y-axis)
 726 and their methylation rate (x-axis), *i.e.* the fraction of non-converted (methylated) C, for each sample
 727 (infection condition and time condition).

728

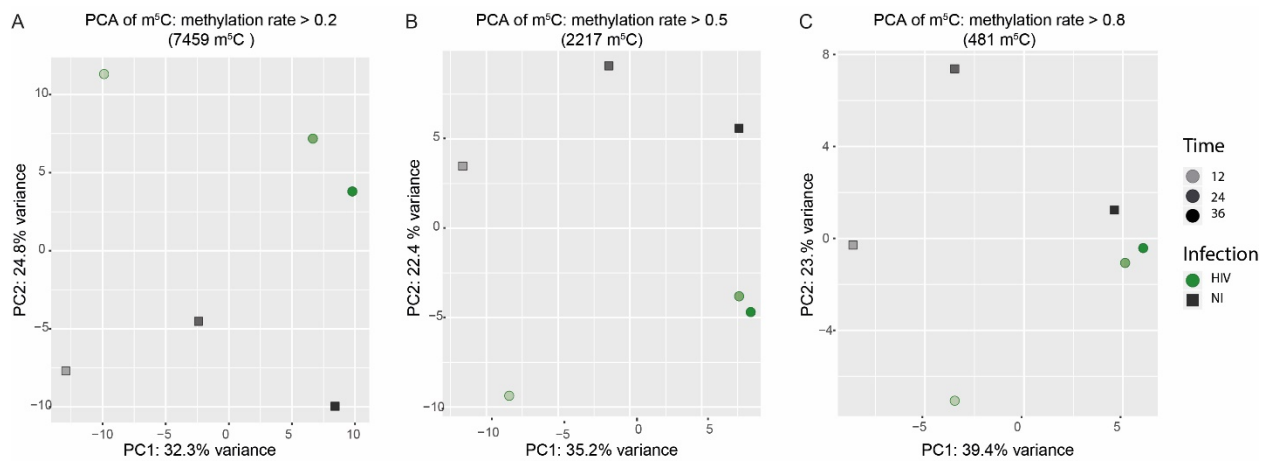
m⁵C distribution within genes



729

730

731 **Figure S6. M⁵C distribution.** Frequency of m⁵C methylation in each sample along genes, normalized by
732 their gene length. Histogram plots showing on the x-axis genes normalized for their length and divided
733 into 30 bins, and for each bin fraction of the gene, the number of m⁵C residues weighted for the
734 methylation rate.



735

736

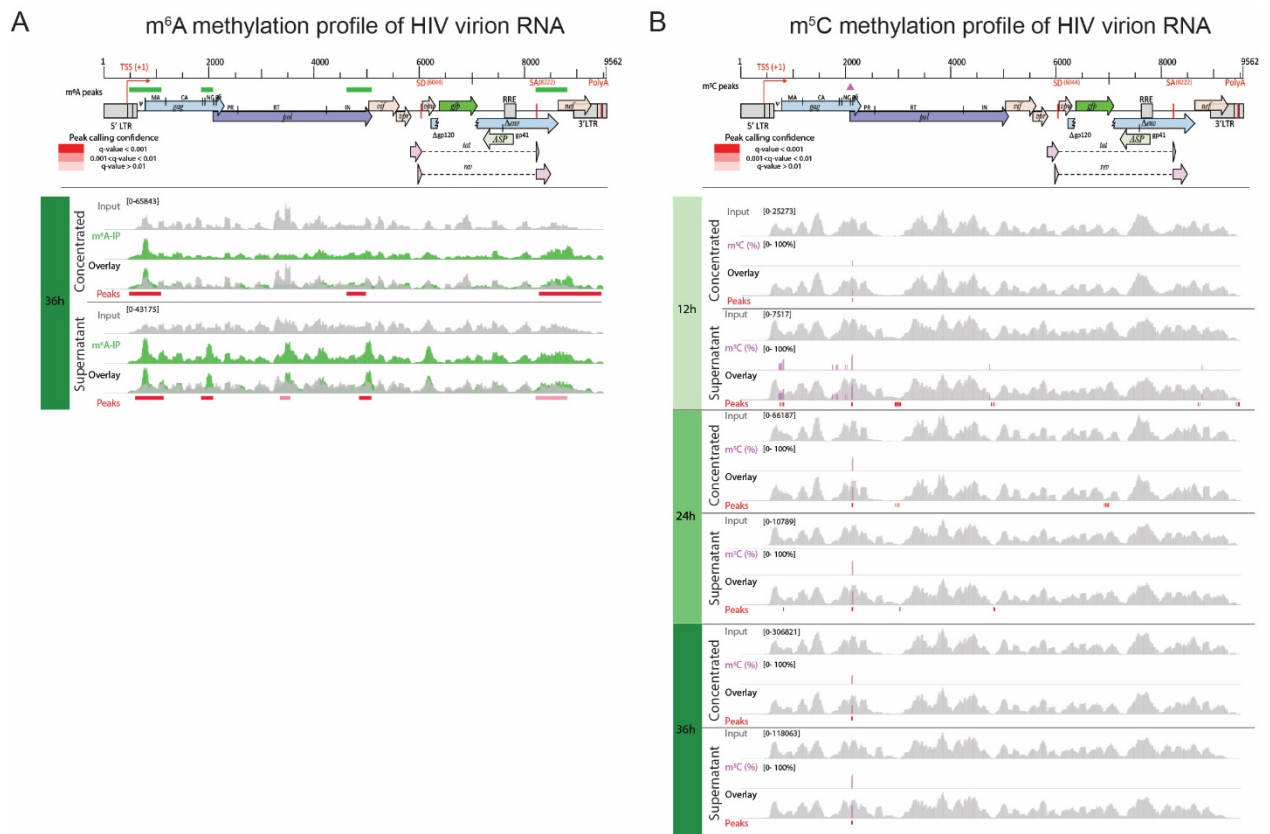
737 **Figure S7. PC analysis of m⁵C across samples according to methylation rate.** Different filters for

738 methylation were considered: methylation rate >20% (A), >50% (B) and >80% (C). HIV-infected samples

739 are represented as green filled circles, non-infected samples as grey squares. Timepoints are depicted by

740 color shading. HIV transcripts are not included.

741



742

743

744 **Figure S8. m⁶A and m⁵C profile in virions.** Virion RNA was extracted either from concentrated and purified
 745 supernatant (concentrated) or from untouched supernatant (supernatant). HIV genome organization is
 746 depicted on top of the panels and common methylation marks are indicated above the genomes as
 747 horizontal green rectangles (A) or pink triangles (B), respectively. Detailed read coverage is displayed for
 748 each individual sample as tracks below the genome. (A) Identification of m⁶A peaks in HIV virion RNA at
 749 36h post-infection. Input (gray) and m⁶A immunoprecipitated samples (green) are shown. Putative m⁶A
 750 peak calling was performed with MACS2 package after subtraction of the input background (overlay).
 751 Statistically significant peaks are highlighted by a red box, with color shading proportional to the q value
 752 (m⁶A peak track). (B) Identification of m⁵C on HIV virion RNA. Coverage of HIV genome upon conversion
 753 (gray) and detection of m⁵C (pink) are shown. M⁵C are presented as proportion of converted C. Bar height
 754 is proportional to the percentage of methylated C in the reads covering the position. The track height is
 755 set to 100%. M⁵C calling was performed with MACS2 package. Statistically significant residues are
 756 highlighted by a red box, with color shading proportional to the q value.

757

758 **Supplementary Data**

759 Table S1. Normalized gene counts and differential gene expression (DGE) analysis

760 Table S2: List of m⁶A detected peaks

761 Table S3: List of differentially methylated m⁶A peaks

762 Table S4: List of m⁵C detected residues

763 Table S5: List of m⁵C differentially methylated residues

764 Table S6: m⁶A and m⁵C methylation detected in HIV RNA molecules isolated from infected cells

765 Table S7: m⁶A and m⁵C methylation detected in HIV RNA molecules isolated from viral particles

766

769 **References**

770

- 771 1. Boccaletto P, Machnicka MA, Purta E, Piatkowski P, Baginski B, Wirecki TK, et al.
772 MODOMICS: a database of RNA modification pathways. 2017 update. *Nucleic Acids Res.*
773 2018;46(D1):D303-D7.
- 774 2. Davalos V, Blanco S, Esteller M. SnapShot: Messenger RNA Modifications. *Cell.*
775 2018;174(2):498- e1.
- 776 3. Saletore Y, Meyer K, Korlach J, Vilfan ID, Jaffrey S, Mason CE. The birth of the
777 Epitranscriptome: deciphering the function of RNA modifications. *Genome Biol.*
778 2012;13(10):175.
- 779 4. Zhao BS, Roundtree IA, He C. Post-transcriptional gene regulation by mRNA
780 modifications. *Nat Rev Mol Cell Biol.* 2017;18(1):31-42.
- 781 5. Meyer KD, Jaffrey SR. The dynamic epitranscriptome: N6-methyladenosine and gene
782 expression control. *Nat Rev Mol Cell Biol.* 2014;15(5):313-26.
- 783 6. Zaccara S, Ries RJ, Jaffrey SR. Reading, writing and erasing mRNA methylation. *Nature*
784 *Reviews Molecular Cell Biology.* 2019;20(10):608-24.
- 785 7. Shi H, Wei J, He C. Where, When, and How: Context-Dependent Functions of RNA
786 Methylation Writers, Readers, and Erasers. *Mol Cell.* 2019;74(4):640-50.
- 787 8. Lichinchi G, Gao S, Saletore Y, Gonzalez GM, Bansal V, Wang Y, et al. Dynamics of the
788 human and viral m(6)A RNA methylomes during HIV-1 infection of T cells. *Nat Microbiol.*
789 2016;1:16011.
- 790 9. Kennedy EM, Bogerd HP, Kornepati AV, Kang D, Ghoshal D, Marshall JB, et al.
791 Posttranscriptional m(6)A Editing of HIV-1 mRNAs Enhances Viral Gene Expression. *Cell*
792 *Host Microbe.* 2016;19(5):675-85.
- 793 10. Lu W, Tirumuru N, St Gelais C, Koneru PC, Liu C, Kvaratskhelia M, et al. N(6)-
794 Methyladenosine-binding proteins suppress HIV-1 infectivity and viral production. *J Biol*
795 *Chem.* 2018;293(34):12992-3005.
- 796 11. Tirumuru N, Zhao BS, Lu W, Lu Z, He C, Wu L. N(6)-methyladenosine of HIV-1 RNA
797 regulates viral infection and HIV-1 Gag protein expression. *Elife.* 2016;5.
- 798 12. Courtney DG, Tsai K, Bogerd HP, Kennedy EM, Law BA, Emery A, et al.
799 Epitranscriptomic Addition of m(5)C to HIV-1 Transcripts Regulates Viral Gene Expression.
800 *Cell Host Microbe.* 2019;26(2):217-27 e6.
- 801 13. Tirumuru N, Wu L. HIV-1 envelope proteins up-regulate N (6)-methyladenosine
802 levels of cellular RNA independently of viral replication. *J Biol Chem.* 2019;294(9):3249-60.
- 803 14. Mohammadi P, Desfarges S, Bartha I, Joos B, Zangger N, Muñoz M, et al. 24 hours in
804 the life of HIV-1 in a T cell line. *PLoS pathogens.* 2013;9(1):e1003161-e.
- 805 15. Dominissini D, Moshitch-Moshkovitz S, Schwartz S, Salmon-Divon M, Ungar L,
806 Osenberg S, et al. Topology of the human and mouse m6A RNA methylomes revealed by m6A-
807 seq. *Nature.* 2012;485(7397):201-6.
- 808 16. Zhang S-Y, Zhang S-W, Liu L, Meng J, Huang Y. m6A-Driver: Identifying Context-
809 Specific mRNA m6A Methylation-Driven Gene Interaction Networks. *PLOS Computational*
810 *Biology.* 2016;12(12):e1005287.

- 811 17. Zaccara S, Ries RJ, Jaffrey SR. Reading, writing and erasing mRNA methylation. *Nat*
812 *Rev Mol Cell Biol.* 2019;20(10):608-24.
- 813 18. Ciucci T, Bosselut R. Gimap and T cells: a matter of life or death. *Eur J Immunol.*
814 2014;44(2):348-51.
- 815 19. Amort T, Rieder D, Wille A, Khokhlova-Cubberley D, Riml C, Trixl L, et al. Distinct 5-
816 methylcytosine profiles in poly(A) RNA from mouse embryonic stem cells and brain. *Genome*
817 *Biol.* 2017;18(1):1.
- 818 20. Rieder D, Amort T, Kugler E, Lusser A, Trajanoski Z. meRanTK: methylated RNA
819 analysis ToolKit. *Bioinformatics.* 2015;32(5):782-5.
- 820 21. Squires JE, Patel HR, Nousch M, Sibbritt T, Humphreys DT, Parker BJ, et al. Widespread
821 occurrence of 5-methylcytosine in human coding and non-coding RNA. *Nucleic Acids Res.*
822 2012;40(11):5023-33.
- 823 22. Kishimoto N, Iga N, Yamamoto K, Takamune N, Misumi S. Virion-incorporated alpha-
824 enolase suppresses the early stage of HIV-1 reverse transcription. *Biochemical and*
825 *Biophysical Research Communications.* 2017;484(2):278-84.
- 826 23. Terada Y, Yasuda Y. Human immunodeficiency virus type 1 Vpr induces G2
827 checkpoint activation by interacting with the splicing factor SAP145. *Molecular and cellular*
828 *biology.* 2006;26(21):8149-58.
- 829 24. Zhang X, Aida Y. HIV-1 Vpr: a novel role in regulating RNA splicing. *Curr HIV Res.*
830 2009;7(2):163-8.
- 831 25. Hashizume C, Kuramitsu M, Zhang X, Kurosawa T, Kamata M, Aida Y. Human
832 immunodeficiency virus type 1 Vpr interacts with spliceosomal protein SAP145 to mediate
833 cellular pre-mRNA splicing inhibition. *Microbes Infect.* 2007;9(4):490-7.
- 834 26. Kim N, Kukkonen S, Gupta S, Aldovini A. Association of Tat with promoters of PTEN
835 and PP2A subunits is key to transcriptional activation of apoptotic pathways in HIV-infected
836 CD4+ T cells. *PLoS pathogens.* 2010;6(9):e1001103-e.
- 837 27. Vitallé J, Terrén I, Orrantia A, Pérez-Garay R, Vidal F, Iribarren JA, et al. CD300a
838 inhibits CD16-mediated NK cell effector functions in HIV-1-infected patients. *Cell Mol*
839 *Immunol.* 2019;16(12):940-2.
- 840 28. Vitallé J, Terrén I, Gamboa-Urquijo L, Orrantia A, Tarancón-Díez L, Genebat M, et al.
841 Altered Expression of CD300a Inhibitory Receptor on CD4+ T Cells From Human
842 Immunodeficiency Virus-1-Infected Patients: Association With Disease Progression
843 Markers. *Front Immunol.* 2018;9:1709-.
- 844 29. Kim DY, Kwon E, Hartley PD, Crosby DC, Mann S, Krogan NJ, et al. CBFbeta stabilizes
845 HIV Vif to counteract APOBEC3 at the expense of RUNX1 target gene expression. *Mol Cell.*
846 2013;49(4):632-44.
- 847 30. Mousnier A, Kubat N, Massias-Simon A, Ségéral E, Rain J-C, Benarous R, et al. von
848 Hippel Lindau binding protein 1-mediated degradation of integrase affects HIV-1 gene
849 expression at a postintegration step. *Proceedings of the National Academy of Sciences of the*
850 *United States of America.* 2007;104(34):13615-20.
- 851 31. Mueller N, van Bel N, Berkhout B, Das AT. HIV-1 splicing at the major splice donor site
852 is restricted by RNA structure. *Virology.* 2014;468-470:609-20.
- 853 32. Figiel M, Krepl M, Park S, Poznański J, Skowronek K, Gołąb A, et al. Mechanism of
854 polypurine tract primer generation by HIV-1 reverse transcriptase. *Journal of Biological*
855 *Chemistry.* 2018;293(1):191-202.

- 856 33. Kobayashi Y, Zhuang J, Peltz S, Dougherty J. Identification of a cellular factor that
857 modulates HIV-1 programmed ribosomal frameshifting. *J Biol Chem.* 2010;285(26):19776-
858 84.
- 859 34. Ringgaard M, Marchand V, Decroly E, Motorin Y, Bennasser Y. FTSJ3 is an RNA 2' -O-
860 methyltransferase recruited by HIV to avoid innate immune sensing. *Nature.*
861 2019;565(7740):500-4.
- 862 35. Naldini L, Blomer U, Gallay P, Ory D, Mulligan R, Gage FH, et al. In vivo gene delivery
863 and stable transduction of nondividing cells by a lentiviral vector. *Science.*
864 1996;272(5259):263-7.
- 865 36. Didion JP, Martin M, Collins FS. Atropos: specific, sensitive, and speedy trimming of
866 sequencing reads. *PeerJ.* 2017;5:e3720.
- 867 37. Kim D, Langmead B, Salzberg SL. HISAT: a fast spliced aligner with low memory
868 requirements. *Nat Methods.* 2015;12(4):357-60.
- 869 38. Li H, Handsaker B, Wysoker A, Fennell T, Ruan J, Homer N, et al. The Sequence
870 Alignment/Map format and SAMtools. *Bioinformatics.* 2009;25(16):2078-9.
- 871 39. Okonechnikov K, Conesa A, García-Alcalde F. Qualimap 2: advanced multi-sample
872 quality control for high-throughput sequencing data. *Bioinformatics (Oxford, England).*
873 2016;32(2):292-4.
- 874 40. Ewels P, Magnusson M, Lundin S, Käller M. MultiQC: summarize analysis results for
875 multiple tools and samples in a single report. *Bioinformatics (Oxford, England).*
876 2016;32(19):3047-8.
- 877 41. Patro R, Duggal G, Love MI, Irizarry RA, Kingsford C. Salmon provides fast and bias-
878 aware quantification of transcript expression. *Nat Methods.* 2017;14(4):417-9.
- 879 42. Zhang Y, Liu T, Meyer CA, Eeckhoute J, Johnson DS, Bernstein BE, et al. Model-based
880 Analysis of ChIP-Seq (MACS). *Genome Biology.* 2008;9(9):R137.
- 881 43. Martin M. Cutadapt removes adapter sequences from high-throughput sequencing
882 reads. *EMBnetjournal; Vol 17, No 1: Next Generation Sequencing Data Analysis.* 2011.
- 883 44. Shen W, Le S, Li Y, Hu F. SeqKit: A Cross-Platform and Ultrafast Toolkit for FASTA/Q
884 File Manipulation. *PLOS ONE.* 2016;11(10):e0163962.
- 885 45. Tarasov A, Vilella AJ, Cuppen E, Nijman IJ, Prins P. Sambamba: fast processing of NGS
886 alignment formats. *Bioinformatics (Oxford, England).* 2015;31(12):2032-4.
- 887 46. Liao Y, Smyth GK, Shi W. featureCounts: an efficient general purpose program for
888 assigning sequence reads to genomic features. *Bioinformatics.* 2013;30(7):923-30.
- 889 47. Sonesson C, Love MI, Robinson MD.
- 890 48. Tarazona S, Furió-Tarí P, Turrà D, Pietro AD, Nueda MJ, Ferrer A, et al. Data quality
891 aware analysis of differential expression in RNA-seq with NOISeq R/Bioc package. *Nucleic
892 acids research.* 2015;43(21):e140-e.
- 893 49. Love MI, Huber W, Anders S. Moderated estimation of fold change and dispersion for
894 RNA-seq data with DESeq2. *Genome Biology.* 2014;15(12):550.
- 895 50. Ross-Innes CS, Stark R, Teschendorff AE, Holmes KA, Ali HR, Dunning MJ, et al.
896 Differential oestrogen receptor binding is associated with clinical outcome in breast cancer.
897 *Nature.* 2012;481(7381):389-93.
- 898 51. Zhu LJ, Gazin C, Lawson ND, Pagès H, Lin SM, Lapointe DS, et al. ChIPpeakAnno: a
899 Bioconductor package to annotate ChIP-seq and ChIP-chip data. *BMC Bioinformatics.*
900 2010;11(1):237.

- 901 52. Robinson MD, McCarthy DJ, Smyth GK. edgeR: a Bioconductor package for differential
902 expression analysis of digital gene expression data. *Bioinformatics* (Oxford, England).
903 2010;26(1):139-40.
- 904 53. BJ T. universalmotif: Import, Modify, and Export Motifs with R. R package version
905 1.0.22, <https://github.com/bjmt/universalmotif>. 2019 [
906 54. Bailey TL. DREME: motif discovery in transcription factor ChIP-seq data.
907 *Bioinformatics*. 2011;27(12):1653-9.
- 908 55. Bailey TL, Elkan C. Fitting a mixture model by expectation maximization to discover
909 motifs in biopolymers. *Proc Int Conf Intell Syst Mol Biol*. 1994;2:28-36.
910